UNIVERSITÀ
DI TORINO

Università degli Studi di Torino

Corso di Laurea Grau de Química

Manufacturing of paper-based electrochemical sensor

Tesi di Laurea

Relatore
Prof. Fabrizio Sordello

Candidato
Guillem Gassol Moreno

Anno Accademico 2022/2023

First of all, I would like to thank Fabrizio Sordello for giving me the opportunity to work on his project and for his guidance and help throughout the development of this work. I would also like to thank my family and my partner for their unconditional support during my time away from home.

CONTENTS:

1. INTRODUCTION AND ABSTRACT 2

2. EXPERIMENTAL SECTION 7

2.1. Reagents 7
2.2. Instrumentation and software 7
2.3. Synthesis of conductive ink 7
2.3.1. Synthesis of nitrocellulose 7
2.3.2. Manufacture of nail polish 7
2.3.3. Ink production 8
2.4. Sensor manufacturing 8
2.4.1. Sensor design 8
2.4.2. Stencilling and painting of the electrodes 9
2.4.3. Sensor modifications 11

3. RESULTS AND DISCUSSION 12

3.1. Optimisation and evaluation of sensor characteristics 12
3.1.1. Sensor design 12
3.1.2. Sensor size 16
3.1.3. Type of stencil used to paint the electrodes 20
3.2. Humidity sensing 27
3.3. Light incidence sensing 31
3.3.1. Potentiometric measurements 32
3.3.2. Current measurements 44
3.3.3. Results comparation 48

4. CONCLUSIONS 54

5. REFERENCE AND NOTES 55

1. INTRODUCTION AND ABSTRACT

In recent years, the development of analytical strategies has led to an evolution of sustainable and low-cost procedures. A very good example of this is paper-based chemical and biological sensors, which offer several advantages such as ease of use, flexibility, small size, and the ability of paper to absorb and retain liquids. But, without a doubt, what makes them most attractive is the simplicity of their fabrication. This, apart from being an environmentally friendly alternative and making them very affordable, allows us the possibility of customizing them for specific uses.

In this work, the intention is to develop from scratch a handmade electrochemical sensor with graphite and silver ink electrodes. This device must be able to work even immersed in a solution and give results in a series of electrochemical measurements. We will synthesize as many of the compounds as we need and adapt the fabrication to the materials that we have. In addition, we will try a modification to specify the sensitivity of the device.

RESULTS AND DISCUSSION (3.)

To optimise the fabrication of our device and to test the different possibilities it offers, we will carry out a series of analyses. Through electrochemical measurements, we will try to determine the best conformation for our sensor, and its sensitivity to changes in relative humidity and we will test some modifications in its composition to distinguish periods of light incidence at different intensities.

Optimisation and evaluation of sensor characteristics (3.1.)

In the development of our device, we have seen different conformations for its manufacture. In this section, we want to study the influence of their most important characteristics, which are those concerning the hydrophobic barrier that delimits the working area, the size of the device, and the type of stencils used to paint the electrodes. Here we will analyse the hydrophobic barrier of the device and the type of stencils.

We have used two types of designs throughout our experience which use two different types of hydrophobic barrier. Design 1 consists of two parts, a single piece of filter paper and a paraffin layer. The paraffin layer, after being heated and embedded into the sensor, delimits the working area. This design, although simple to manufacture, presents a problem in its ability to retain solutions in the delimited area, with the risk of short-circuiting the device when the electrolyte reaches the connectors. The other design (Design 2) consists of three parts, two made of filter paper and one of paraffin. The paraffin part connects the two pieces of paper and acts as a hydrophobic barrier. The conformation allows us to keep the solution under study in the working area for an unlimited time, which should lead to better results and extend the life of the sensor. The only drawback of this sensor is that it requires more manufacturing time. Figure 1.1 shows a device with design 1 after 10 minutes with its working area immersed in solution (left), and a device with design 2 after 1 hour with its working area immersed in solution (right).

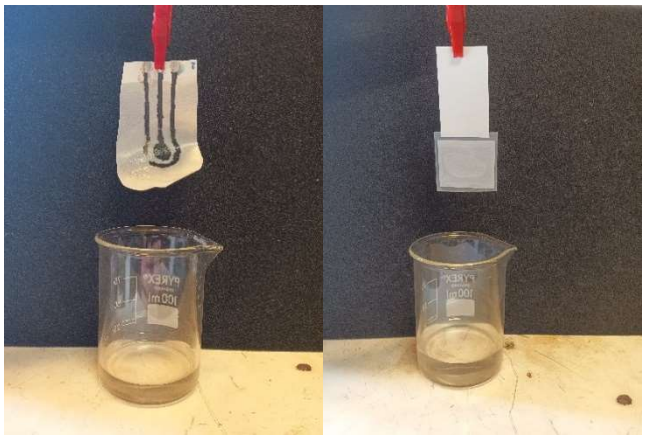

Figure 1.1. Device with design 1 after 10 minutes immersed in solution (left). Device with design 2 after 1 hour immersed in solution (right).

The last feature of sensor fabrication that we will study is the type of stencil we will use to paint the electrodes. During our work we will use two different types of stencils, one made of office paper and the other made of the polymer PLA (PolyLactic Acid). The paper ones are printed on a DIN A4 sheet and only require a cutter to cut out the relief of the electrodes and an inkjet printer. Their main disadvantage is that they deteriorate with use, which affects the shape of the electrodes, and the poor adhesion to the sensor's filter paper, which causes the ink to seep under the stencil easily. On the other hand, the PLA (PolyLactic Acid) stencils offer greater strength and rigidity, which allows the electrodes to be painted wider and more defined. The manufacturing process becomes more reproducible Their main disadvantage is that they require a 3D printer. Sensor 9.2 was tested in a solution of 1mM $K_3Fe(CN)_6$ and 0.1M KCl, where we observed two reversible current peaks, at 0.2 (anodic scan) and 0.1V (cathodic scan), which we attributed to K_3 $Fe(CN)_6$ (Figure 1.2).

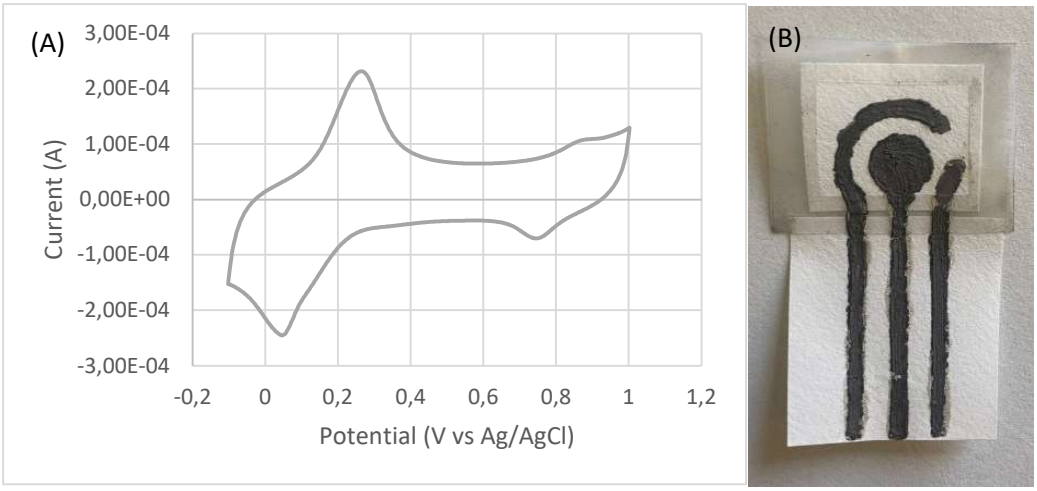

Figure 1.2. (A) Cyclic voltammetry of sensor 9.2 recorded at 0.05V s^{-1} in 1mM of $K_3Fe(CN)_6$ and 0.1M of KCl (solution 1). (B) Sensor 9.2 which uses Design 2 and PLA (PolyLactic Acid) stencil.

Humidity sensing (3.2.)

To study the possibilities offered by our device, we will test its sensitivity to relative humidity. In this experiment, we will use a solution of $CaCl_2$, a compound with hygroscopic properties. Varying its concentration, we will be able to control the relative humidity from 30%

to 90% in a container (desiccator) where our sensor will be located. By performing chronoamperometries, we expect to see an increase in the electric current as the humidity level rises.

The average values of electric current obtained for each relative humidity are shown in Table 1.1. Recoveries are also reported to test the recognition and prediction ability of the regression curve. The first recovery column in Table 1.1 assesses if the regression curve can recognize the % RH employed to build the curve, while the second column evaluates the prediction ability, as those recovery values were calculated with the regression curves obtained without the RH value under consideration.

Table 1.1. Average values of electric current obtained for each % relative humidity level and % $CaCl_2$ mass concentration.

Relative humidity (%)	Average stabilised current (A)	$CaCl_2$ mass concentration (%)	Recovery %[a]	Recovery %[b]
30	6,33E-10	44,36	58,90	-1,68
40	5,8E-9	39,62	121,85	128,22
50	9,37E-9	35,64	110,94	113,18
60	1,62E-8	31,73	105,25	106,13
70	2,72E-8	27.40	100,63	100,85
80	4,53E-8	22,25	96,96	95,87
90	8,72E-8	14,95	96,38	93,80

a Calculated as the ratio between RH calculated with the regression curve of Figure 1.3 and nominal RH.

b Calculated as the ratio between RH calculated with the regression curve obtained without the value under consideration and nominal RH.

Figure 1.3 reports the current values obtained as a function of time at different % RH and the calibration curve of the average current values vs % RH. The curve is exponential with equation $y=1.795E\text{-}10e^{0.0713x}$ and $R^2 = 0.9934$.

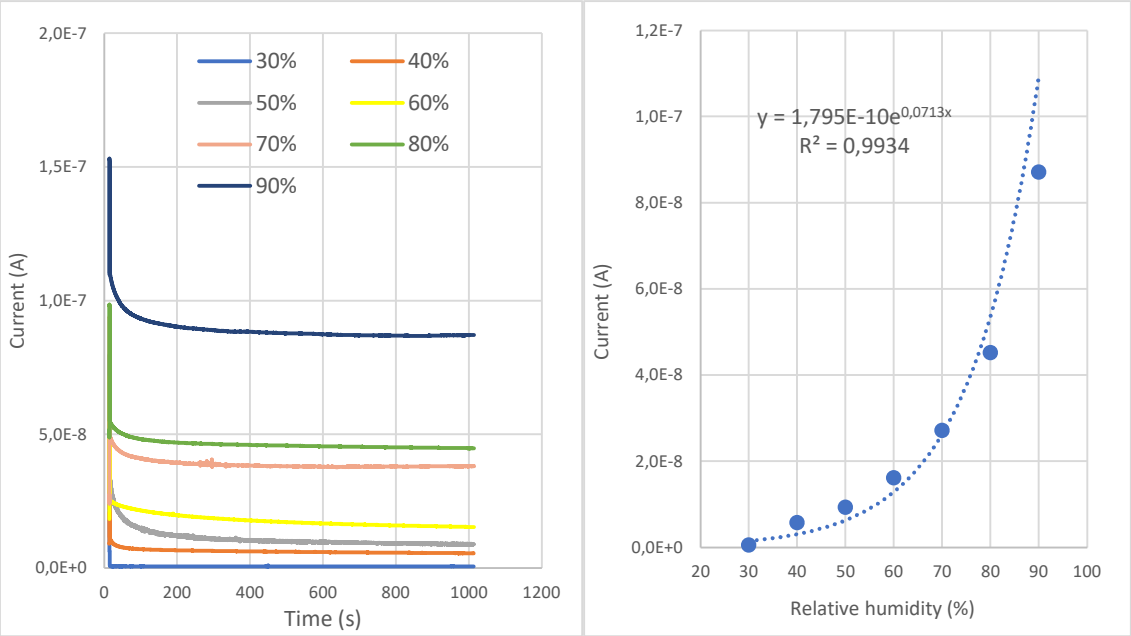

Figure 1.3. Chronoamperometries at different % RH values (left). Calibration curve of average current values vs %RH (right).

Light incidence sensing (3.3.)

Paper-based sensors offer the possibility to specify their sensitivity to both, analytes, and physical properties. In our work, we want to test the photocatalytic properties of TiO_2 by using it as a modifier for our device to distinguish periods of indecency and non-incidence of light at different intensities. When TiO_2 is irradiated with visible light of energy equal to or higher than the energy of the forbidden band, the electrons of its valence band are excited to its conduction band, leaving holes in the valence band. This results in an increase of the conductivity and a decrease of the open circuit potential in the sensor, which we can quantify through chronoamperometry and chronopotentiometry, respectively. We will use two types of modified sensors, those that contain the TiO_2 on the surface of the working electrode and those that contain it in the ink of this same electrode. Table 1.2 shows the type of modification and the sensor number.

Table 1.2. Type of modification, sensor number and modification specifications.

Type of modification	Sensor number and modification		
On the WE surface	Sensor 7: water + TiO_2	Sensor 13: water + TiO_2; silver electrodes	Sensor 8: nail polish + acetone + TiO_2
In the ink of the WE	Sensor 11: 2% TiO_2 in the ink	Sensor 10: 10% TiO_2 in the ink	Sensor 12: 50% TiO_2 in the ink

We noticed that chronopotentiometry was an ineffective tool to sense irradiation with this kind of device. In fact, the large resistance of the printed electrodes compared with conventional electrodes, made open circuit monitoring noisy and not reproducible, due to drift, probably due to charging of the WE under irradiation. Therefore, we decided to monitor the current, instead of the open circuit potential, which appeared to be noisy on electrodes printed on paper. Chronoamperometries were recorded in a two-electrode configuration with a cell voltage of 0.5 V. Starting again with Sensor 7, we obtained very good results (Figure 1.4 left). The current under irradiation significantly increases and tends to stabilise rapidly, also in the subsequent dark period. In addition, the larger the photon flux, the larger the photocurrent. Sensor 10 shows the same results, although with a much lower signal compared to Sensor 7. The measurements with Sensor 11 only show the signals of irradiation above 1.8 $W\text{-}m^{-2}$, which shows that this sensor is less sensitive than the ones tested so far. The response to all the irradiation intensities to which we subjected it shows signals equal to those obtained with Sensor 7. As the last measurement, we test the Sensor 12. The peaks are easily distinguishable and of high reproducibility, although the measurement is affected by noise in the middle of the analysis (Figure 1.4 right).

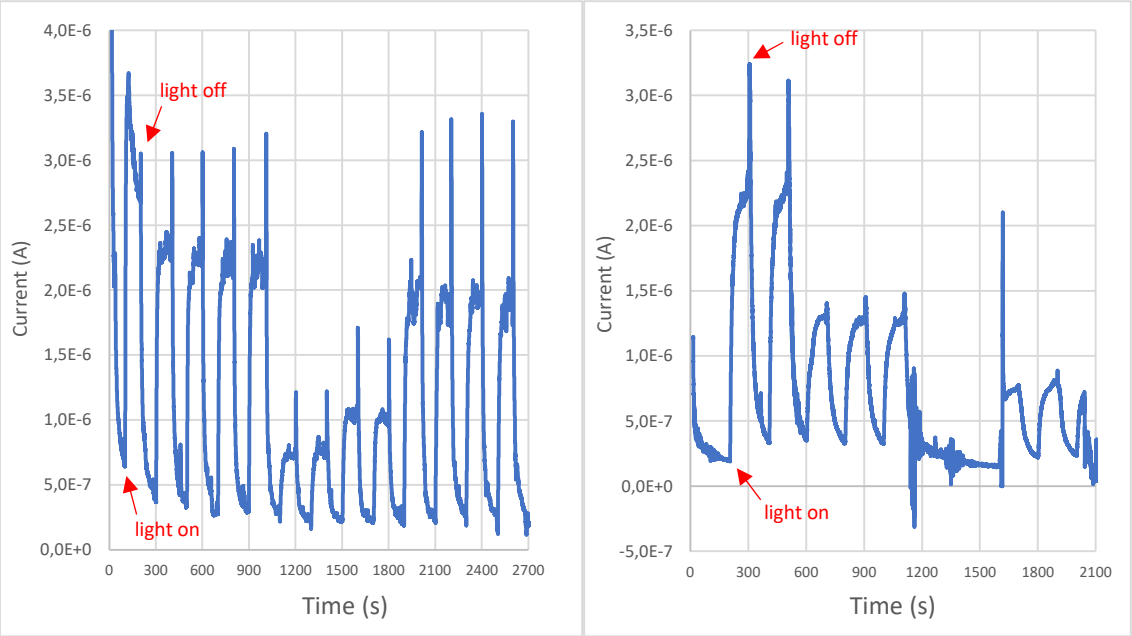

Figure 1.4. Chronoamperometry of Sensor 7, alternating irradiance, and dark periods. Light intensity was 26 W m-2 from 0 s to 1100 s and from 1900 s to 2200, 1.8 W m-2 from 1100 s to 1500 s and 5.4 W m-2 from 1500s to 1900s (left). Chronoamperometry of Sensor 12, alternating irradiance, and dark periods. Light intensity was 26 W m-2 from 0 s to 600 s, 5.4 W m-2 from 600 s to 1600 s and 1.8 W m-2 from 1600s to 2100s (right).

2. EXPERIMENTAL SECTION

2.1. REAGENTS

Graphite powder (1-2 micron), cellulose microcrystalline powder, toluene, butyl acetate, ethyl acetate, HNO_3 (60%), H_2SO_4 (80%), $K_3Fe(CN)_6$, $CuSO_4$, KCl, $CaCl_2$ were acquired from Sigma-Aldrich. Laboratory film, Parafilm "M" from Bemis. Filter paper (qualitative, 150 mm) from Whatman. Silver conductive paint from RS PRO. Household bleach (3.5% NaClO) was purchased from Carrefour. Acetone and TiO_2 particles. All reagents were of analytical purity.

2.2. INSTRUMENTATION AND SOFTWARE

The instruments used to carry out these experiments are the Agilent 34401A 6 ½ Digital Multimeter, to check the electrical resistance of the electrodes and the Metrohm / Eco Chemie Autolab PGSTAT12 Potentiostat/Galvanostat to carry out the electrochemical measurements. The software used for this last instrument is the NOVA version 1.8.

2.3. SYNTHESIS OF CONDUCTIVE INKS

The electrodes of the sensors that we will make are made of conductive ink. In our case, we will use two types of ink, silver ink, which is of commercial origin, and graphite ink that we will make ourselves. This graphite ink consists of three components: graphite, which will be the conductive medium of the ink; nail polish (also made by us) so that the ink sticks to the surface of the paper and acetone to dissolve the mixture and give it a more liquid texture so that it spreads more easily. The process is divided into three main parts which are the synthesis of nitrocellulose, the main ingredient of the nail polish, the manufacture of the nail polish itself, and finally the elaboration of the ink.

2.3.1. Synthesis of nitrocellulose

To carry out this synthesis we will need the main component, cellulose. By means of a nitration process with HNO_3, we will obtain the desired compound. First, we mix 30 ml of HNO_3 at 60% and 80 ml of H_2SO_4 at 98% in a beaker. We will have to wait until this mixture cools down, so it is useful to leave the beaker in an ice bath with water to accelerate the process. Once the solution has reached a temperature of 20°C, add 5 g of cellulose to the vessel. Wait for 1 hour and then wash the product obtained 3 to 5 times with water. Then we introduce it into a saturated solution of sodium bicarbonate to neutralise any remaining acid and finally, we wash the resulting product once more with water and leave it to dry at room temperature. Once dry, it should have the same appearance as the initial cellulose, but its colour will have turned yellowish.

2.3.2. Manufacture of nail polish

With the nitrocellulose ready, we can now prepare the nail polish. For its manufacture we have adapted a recipe by eliminating the minority components and using only the 4 main ingredients in the following proportions by mass: 34% toluene, 31% butyl acetate, 17% ethyl acetate, and 18% nitrocellulose.

For our process, we use 1.8 grams of nitrocellulose to which we add 3.9 ml of toluene, 3.5 ml of butyl acetate, and 1.9 ml of ethyl acetate. Mix the compounds by hand for at least 20 minutes and with the aid of the ultrasonic bath, until no more nitrocellulose pieces are observed, and the resulting product has a viscous texture. It is advisable to keep the resulting product well covered to prevent it from drying out and having to re-incorporate the solvent mixture.

2.3.3. Ink production

Now we have the three main parts, so we can finally prepare the ink. All we need to do is to mix the graphite powder and the freshly prepared nail polish together in a 50/50 mass ratio. It is important for the nail polish to be as fresh as possible otherwise there is a risk that the ink will not adhere easily. In our case, we mixed 1.6 g of each of the components. Finally, we add the acetone. For the mass that we are using, only 3 ml of acetone is enough, but it also depends on the desired texture. Once you have added this last component, mix until you see a homogeneous substance with no solid parts, and you will have the ink ready. It is recommendable to use it just after making the ink to prevent it from drying out, in the case that this happens, you only need to add a little more of the solvent and acetone mixture.

2.4. SENSOR MANUFACTURING

In the manufacturing of our devices, we can distinguish several important steps, referring to their fabrication and the optimisation of their use. That is why we will distinguish in the manufacturing section three main parts. The first one is about the design of the electrode support and the hydrophobic barrier surrounding the working area. The second is related to the type of stencil used to paint the electrodes on the surface of the paper and the procedure to follow to do so. And the last one is related to the variations we have made on the sensor in order to modify its analytical purpose.

2.4.1. Sensor design

In our experiences, we have used two different designs, both of which use the same materials, filter paper and paraffin.

The first design is the simplest. It consists of only two parts, a strip of filter paper large enough to fit the electrodes (taking into account that the sensor will measure more or less 5x3.5 cm, we will use a strip slightly larger than these dimensions which we will then adjust to the desired measurements) and a paraffin box with a hole in the center (preferably square) where the working area will be located. Once we have the two pieces, we will place the paraffin part on one of the ends of the paper. Leave it in the oven at 100ºC for at least half an hour, so that the paraffin impregnates the paper and sticks to it. Keep in mind that when the paraffin is heated, it spreads in all directions, so the hole in the middle has to be big enough to accommodate the working area once the paraffin has passed through the oven. After this waiting time, the electrode support is ready.

The second design is a little more complicated to elaborate, it consists of three initial pieces, a square, which will be the working area of the sensor, of about 2.5x2 cm, a rectangular one where the rest of the electrodes will be painted with dimensions of 4x3.5cm and a piece of Parafilm which will join both pieces of paper and which will serve as a hydrophobic barrier so

that the solution studied does not reach the connectors of the sensor. The three pieces will be joined as shown in Figure 2.1. Once we have all the pieces together, we will seal them using the heat of a hot plate. Bringing the plate to about 200ºC, approaching the instrument briefly close to the heat source, and pressing with the hands should be enough to bring all the parts together and obtain the result shown in Figure 2.1.

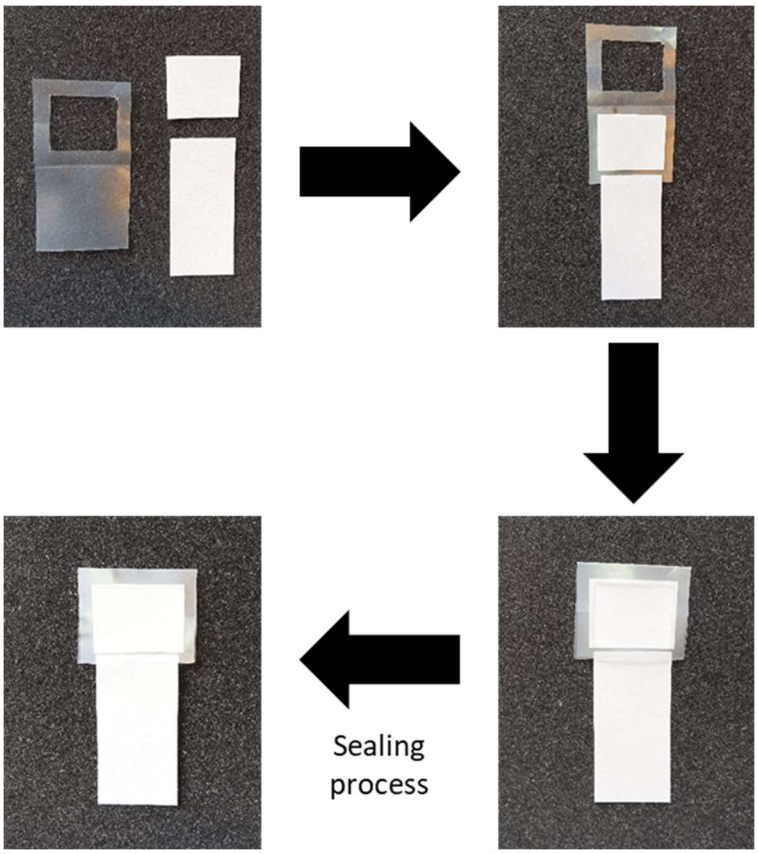

Figure 2.1. Support manufacturing process.

2.4.2. Stencilling and painting of the electrodes

To paint the electrodes on the surface of the paper, we used stencils with the shape of the electrodes, to obtain a better-quality result. During our experience in manufacturing these devices, we have used two different types of materials to support the electrode patterns. In the beginning, we used templates made of paper, printed with an inkjet printer, and with a pattern cut out by hand with a cutter. Later we used templates printed with a 3D printer made of a polymer called PLA (Polylactic Acid). In Figure 2.2 we can see the two types of stencils.

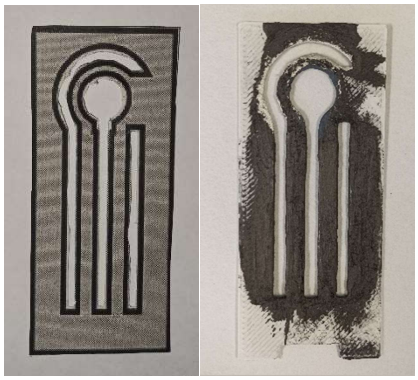

Figure 2.2. Paper stencil (left) and PLA (Polylactic Acid) stencil (right).

The procedure to paint our electrodes over the paper surface is shown in Figure 2.3. Our device consists of two layers of conductive ink (which is why we use two different stencils). The first layer of silver ink and the second layer of graphite ink. The first layer is used to mark the conductive guides of the potentiostat and for our reference electrode, which is why it is the first to be stencilled. It will occupy the first section of the sensor, before reaching the working area. It is important that this condition is met, since otherwise, in the presence of chloride ions and if we work at potentials >0.1V, there could be interference in our measurements due to the oxidation of the metallic silver, following the reaction $Ag + Cl^- \rightarrow AgCl + e^-$. This is why it is advisable to leave a noticeable gap between the end of the silver layer and the working area. To paint it, we will use the corresponding stencil and a brush. Once it is painted, we will put the sensor in the oven for 5 to 7 minutes at 60ºC degrees, so that the ink dries. It is possible that in this procedure the paraffin part of the paper may peel off, in which case it must be glued again with the hot plate before painting the next layer. Once the silver is dry, we will paint the graphite ink layer with its stencil. This will occupy the surface of the previous layer and the part corresponding to the working electrode and the auxiliary electrode. To dry it, follow the same procedure as before.

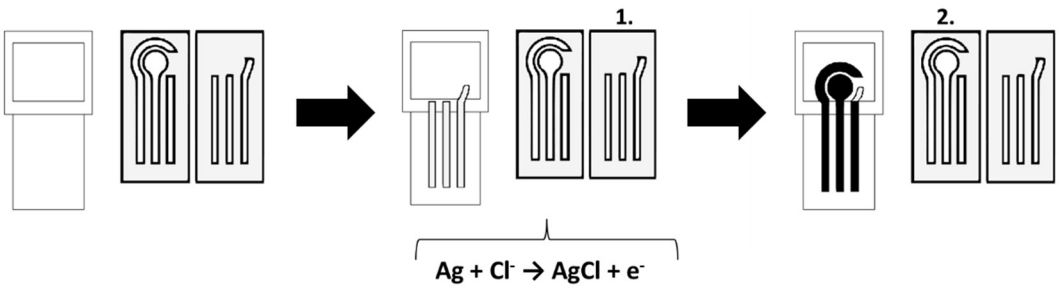

Figure 2.3. Electrode painting process.

Finally, once the electrodes are dry, we will proceed to make the reference electrode. To do this, we will paint the part corresponding to this electrode with bleach for 5 minutes. In this way, we will create a layer of AgCl to obtain our Ag/AgCl electrode.

2.4.3. Sensor modification

TiO_2 is a material with photocatalytic properties. By making some modifications to our sensor, we will test how it responds to the incidence of visible light on its working area. We propose 4 different types of modifications. In the first one, the graphite working electrode will be coated with a mixture of TiO_2 particles in water. The second one will be the same as the first one, but the TiO_2 particles will be in a mixture of acetone and nail polish. The third modification will consist of a sensor with its working electrode composed of graphite ink with different proportions of TiO_2 in it (2%, 10% and 50%). The last modification will consist of a sensor with all its electrodes only painted with silver ink plus a layer of TiO_2 in water on its working electrode.

i) SENSOR 7 (TiO_2 slurry): For this sensor we mix 0.1507 g of TiO_2 with 1ml of water. The resulting product is spread across the width of the working electrode previously covered with graphite ink.

ii) SENSOR 8 (TiO_2 + nail polish + acetone): We mixed 0.3392 g TiO_2, 0.7598 g nail polish and 0.784 g acetone in a vial. The resulting compound is used to coat the graphite working area of the sensor.

iii) SENSOR 10 (graphite + 10% TiO_2): We mix 0.1769 g of TiO_2 with 1.7674 g of our previously prepared graphite ink. The resulting product is a graphite ink with 10.01% TiO_2 particles.

(iv) SENSOR 11 (graphite + 2% TiO_2): 0.1324 g of graphite ink and 0.0031 g of TiO_2 particles are placed in a container. The resulting product is a graphite ink with 2.34% TiO_2 particles.

v) SENSOR 12 (graphite + TiO_2 at 50%): In a container we mix 0.1100 g of graphite ink and 0.0548 g of TiO_2 particles. We obtain a graphite ink product with 49.8% TiO_2 particles.

vi) SENSOR 13 (silver + TiO_2 in water): We painted the three electrodes and all their parts with silver ink. Then we coated their working area with a solution of TiO_2 with water.

3. RESULTS AND DISCUSSION

3.1. OPTIMISATION AND EVALUATION OF SENSOR CHARACTERISTICS

The first study of the electrochemical characteristics will be carried out through cyclic voltammetry. In this way, we will try to evaluate several characteristics of our sensors, like their design (e.g. the type of hydrophobic barrier used to limit the sensing area, the conductive ink employed, etc…), the size of the sensor and the way we shape the electrodes, whether we use paper or 3D printed polymer templates.

3.1.1. Sensor design

For this study, two different designs were used. The first (Design 1) consists of two parts, a single piece of filter paper and a paraffin layer. The paraffin layer, after being heated and embedded in the sensor, delimits the working area. Examples of these sensors are numbers 1, 2, and 3. We will analyse the results of these three sensors together because all have been manufactured with the same ink and the same procedure and a paper stencil has been used to paint the electrodes.

The main problem with this design is the inability to retain the solution under study in the working area (This can be seen in Figure 3.1). On the one hand, this means a reduction in the volume of analyte on which the measurement is taken, and, on the other hand, it reduces the time during which the measurement can be taken, because when the solution reaches the connectors of the potentiostat (or any instrument) the device is short-circuited. Therefore, it only allows us to work with small volumes of electrolyte and never with the sensor immersed in the solution. In this case, after 10 minutes we observe how the solution reaches the connectors, in addition to increasing the possibility of deterioration of the sensor, due to the wetting of the paper.

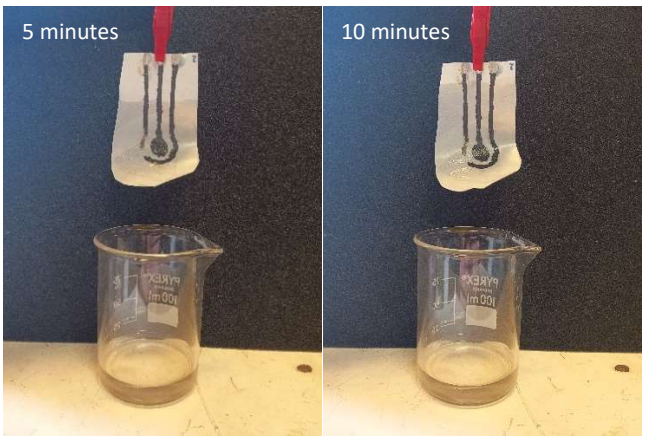

Figure 3.1. Sensor with design 1 after 5 and minutes immersed in solution.

However, with this design, we tested how the sensors perform when carrying out an electrochemical measurement such as cyclic voltammetry. For these tests, we employed a three-electrode setup and first, we studied the behaviour of the sensor in the presence of $K_3Fe(CN)_6$.

We started with Sensors 1 and 2, a volume of 800 µL and a solution of 1 mM $K_3Fe(CN)_6$ and 0.1 M KCl, which we will refer to as solution 1.

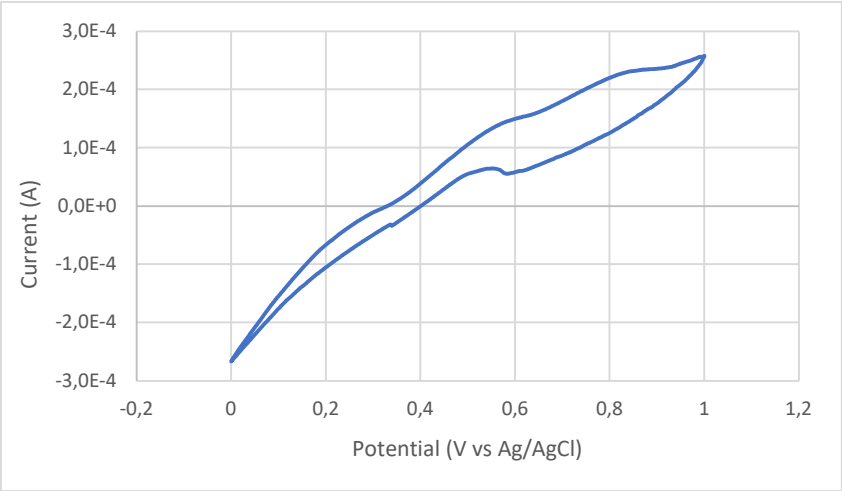

Figure 3.2. Cyclic voltammetry of Sensor 1 recorded at 0.05 V s^{-1} in 1 mM $K_3Fe(CN)_6$ and 0.1 M KCl (solution 1).

We made three measurements at different scan rates, namely 0.2 V s^{-1}, 0.1 V s^{-1}, and 0.05 V s^{-1}. The result at the lowest scan rate is reported in Figure 3.2**.** The voltammogram does not show reversible redox features, which could be attributed to $K_3Fe(CN)_6$. There are broad and low-intensity current peaks at 0.55 and 0.8 V in the anodic scan and 0.6 V in the cathodic scan. The two peaks at 0.6 and 0.8 V are attributed to non-complexed iron.

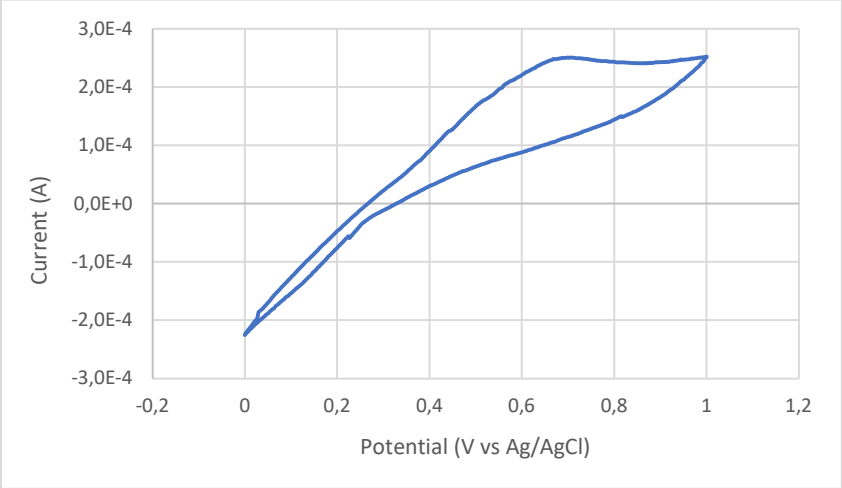

Figure 3.3. Cyclic voltammetry of Sensor 2 recorded at 0.05 V s^{-1} in 1 mM $K_3Fe(CN)_6$ and 0.1 M KCl (solution 1).

For Sensor 2 (3.3) the result is similar, as neither in this case did we observe any peak that could be attributable to the $K_3Fe(CN)_6$. We performed the same experiment with sensor 3, this time using 600 µL of solution 1 (Figure 3.4).

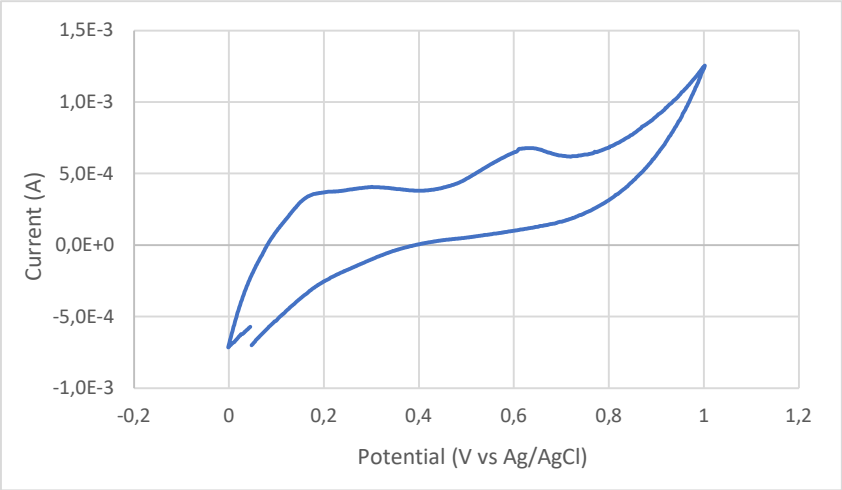

Figure 3.4. Cyclic voltammetry of Sensor 3 recorded at 0.05 V s^{-1} in 1 mM $K_3Fe(CN)_6$ and 0.1 M KCl (solution 1).

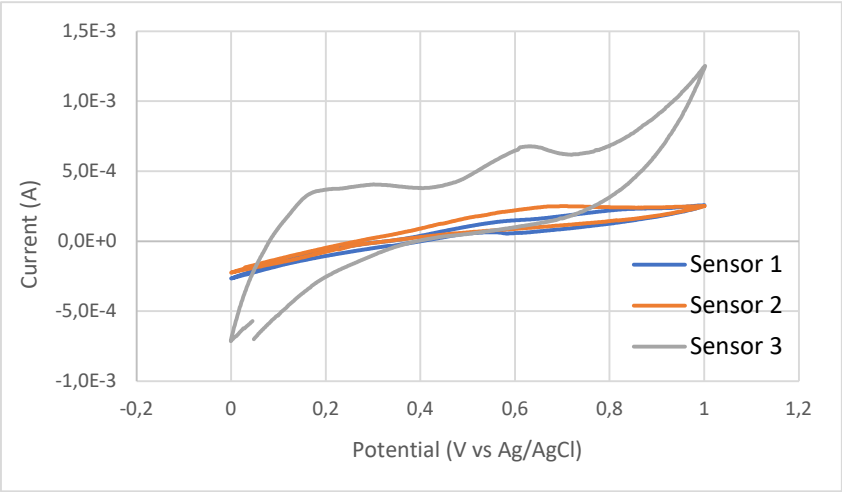

Figure 3.5. Comparation of voltammetry obtained with sensor that use design 1.

Again, the measurement obtained does not show any current peak due to $K_3Fe(CN)_6$. Conversely, we observed a significant increase in current, being sensor 3 signals almost five times higher compared to Sensors 1 and 2 (Figure 3.5. Comparation of voltammetry obtained with a sensor that uses design 1.). However, because of the poor ability of this sensor design to retain a volume of analyte in its working area, we cannot attribute this increase in current to the difference in solution volume used in the different experiments. The results demonstrate that Design 1 is not suitable for this type of electrochemical characterisation.

Design 2 is manufactured in a different way. It consists of three parts, two pieces of filter paper and one piece of paraffin. The paraffin part is used to connect the two pieces of paper. What this design allows us to do is to keep the studied solution in the working area for an unlimited time, which should lead to better results and extend the life of the sensor.

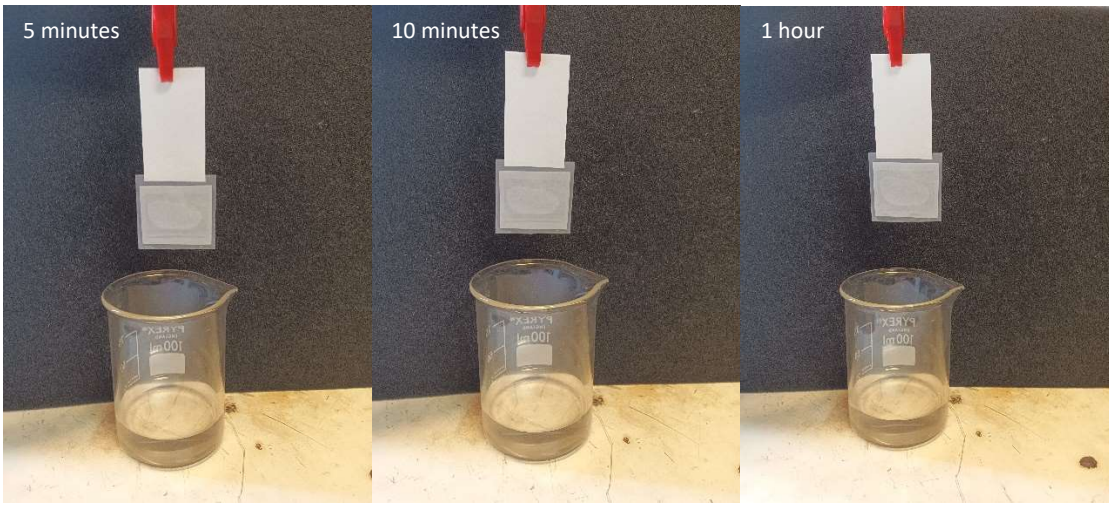

Figure 3.6. Sensor with design 2 after 5 minutes, 10 minutes and 1 hour immersed in solution.

The sensors with Design 2 are all from Sensor number 4 onwards. As in this case, we are only evaluating the efficiency of the design we will not compare and analyse the results of all the sensors with this conformation and we will only do it with Sensor 4. The solution we will study will be solution 1 as before, but in this case, we will also carry out some measurements with solution 1 plus a concentrated solution of $K_3Fe(CN)_6$ 10 mM (we will refer to this solution as solution 2). All the following measurements are taken at a scan rate of 0.05 V s^{-1}.

We will first analyse the functioning of the sensor itself and the influence of the analyte concentration on the results, and then compare them with those obtained from the sensors with Design 1. The setup used is the same as before, and now we will use 500 µL of solution 1 for one measurement and 500 µL of solution 1 plus 100 µL of solution 2 for the other measurement. We work with smaller volumes to avoid the solution studied overflowing the working area of the sensor, as this is now delimited.

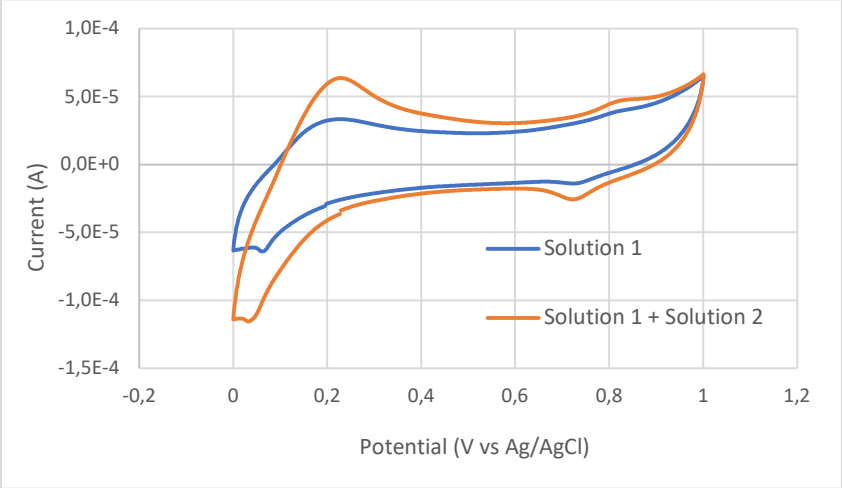

Figure 3.7. Comparation between cyclic voltammetry of Sensor 4 recorded at 0.05 V s^{-1} in 1 mM $K_3Fe(CN)_6$ and 0.1 M KCl (blue) and in 1 mM $K_3Fe(CN)_6$ and 0.1 M KCl + 10 mM of $K_3Fe(CN)_6$ (orange).

In this case, the results are somewhat better than before. For both solutions, we observe two peaks at 0.2 and 0.8 V in the anodic scan and what could be a very low signal peak at about

0.1 V and another at about 0.7 V in the cathodic scan. The peaks at 0.2 and 0.1 V could be due to the reversible redox characteristics of the studied specie. We can also see the effect of the concentration, observing a higher signal in the measurement taken with solution 2.

With the results of this design, we can now compare them with those of the previous design. To do so, we will use the data obtained with Sensor 1 versus those obtained with Sensor 4 when analysing solution 1, for the conditions to be as similar as possible.

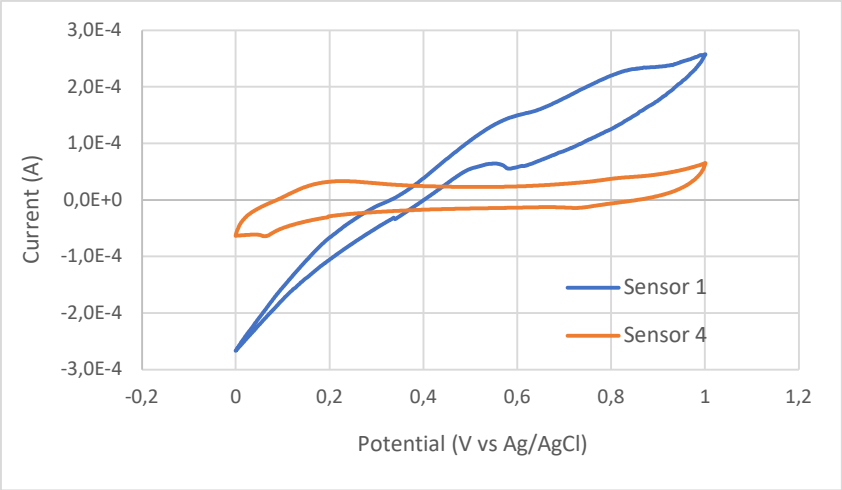

Figure 3.8. Comparation between cyclic voltammetry of Sensor 1 (design 1) and sensor 4 (design 2).

What we can notice is that while Sensor 4 shows the conventional signal, with capacitance current, expected for this type of device, Sensor 1 shows an ohmic behaviour due to the wetting of the paper during the analysis, which causes the electrodes to short-circuit.

Although the results with Sensor 4 do not show a high intensity for the expected signals, we can conclude that design 2 is better. It shows even a slight redox behaviour of the species studied, it allows measurements to be taken for a longer time and it extends the lifetime of the sensor. We can also conclude that for better results it is advisable to work in concentrations higher than 1 mM, at least for this solution.

3.1.2. Sensor size

Another factor to consider in the design of the sensor is its size. In principle, the smaller the size, the better the results, since the ratio between the volume studied and the sensor's working area would be greater, which means that we would be able to analyse more analyte volume in relation to the sensitive area of our device. Having said that, we think that the smaller size option will be the best, but there is another element to consider, which is the manufacturing cost, considering that the sensors are manufactured by hand, the fact that they are smaller adds more difficulty. That is why we are going to analyse the results with two sensors of different dimensions. These have been manufactured in the same way (Design 2 is already applied in these), with paper stencils to paint the electrodes and the same inks. Specifically, we will study the results of Sensor 5 (3.5cm x 2cm) and Sensor 4 (5cm x 2.5cm), which we have seen previously. For the following results shown and compared the scan rate will be always 0.05 V s^{-1}.

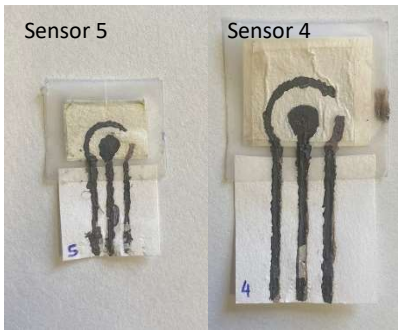

Figure 3.9. Size comparation in scale between Sensor 5 (left) and Sensor 4 (right).

We will start by analysing the results of Sensor 5, with a three-electrode setup and solution 1. Thanks to the smaller size of this sensor, it allows us to work with smaller volumes, which is an advantage when analysing real matrices. Even so, we do not know its efficiency depending on the volume analysed, therefore, we will perform different measurements starting from 50 µL.

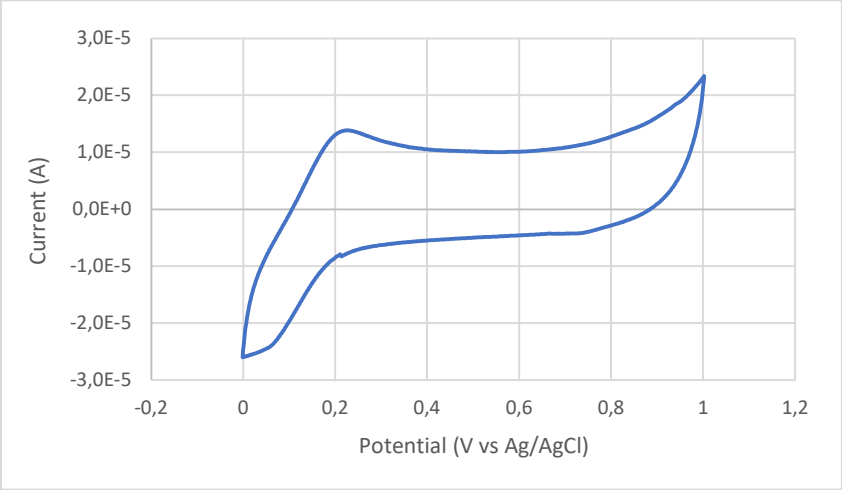

Figure 3.10. Cyclic voltammetry of Sensor 5 recorded at 0.05 V s^{-1} in 1 mM $K_3Fe(CN)_6$ and 0.1 M KCl (solution 1).

We can see that at this volume the sensor does not work correctly, and the results are not as expected. In the anodic scan, there is a peak at 0.2 V and for the cathodic scan, there are no recognisable peaks. Even so, we do not see the peaks that we had seen until now between 0.6 V and 0.8 V corresponding to non-complexed iron, which, although they do not correspond to the species studied, its absence indicates that the device is not working as well as before. That's why we performed a measurement with twice the volume of the same solution. The voltammogram obtained is shown in Figure 3.11.

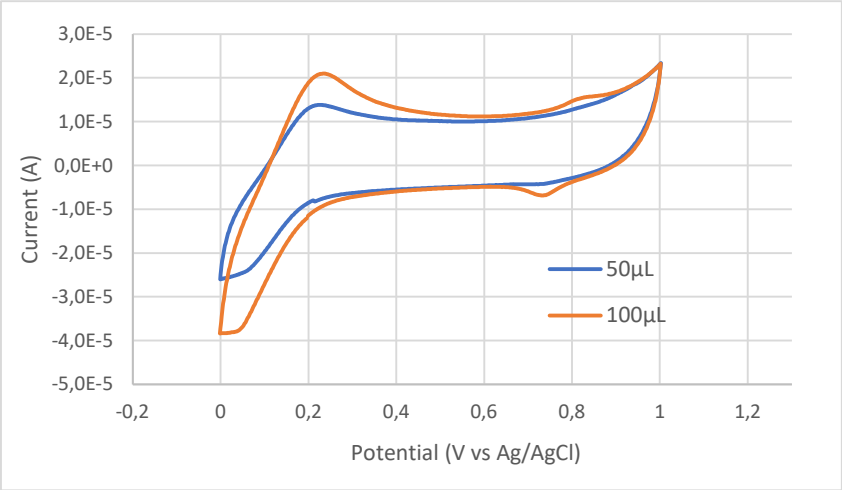

Figure 3.11. Cyclic voltammetry of Sensor 5 recorded at 0.05 V s^{-1} in 1 mM $K_3Fe(CN)_6$ and 0.1 M KCl (solution 1) using two different volumes of 50 and 100 µL.

We can observe that the signal increases throughout the measurement. Now, we can see two peaks in the anodic scan at 0.2 and 0.8 V and one peak at 0.75 V in the cathodic scan. The pair at 0.8 and 0.75 V is attributed to the non-complexed iron. Even so, we try doubling the analysed volume again and the results are shown in Figure 3.12.

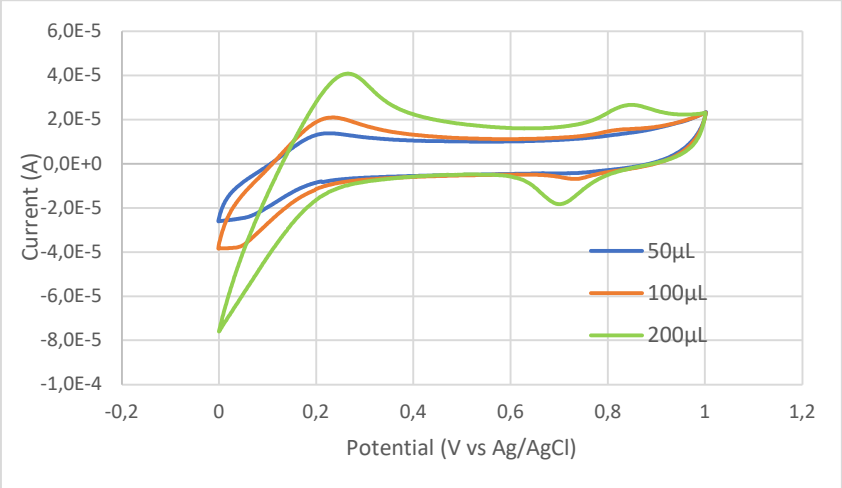

Figure 3.12. Comparation of cyclic voltammetry of Sensor 5 recorded at 0.05 V s^{-1} in 1 mM $K_3Fe(CN)_6$ and 0.1 M KCl (solution 1) using two different volumes of 50, 100 and 200 µL.

This measurement clearly shows the influence of volume on the results obtained. The signal at 200 µL is much larger than the two previous ones and with more pronounced peaks. We still do not see any features attributable to the reversible redox characteristics of $K_3Fe(CN)_6$. Now we can see the peaks between 0.6 V and 0.8 V, which indicates that the sensor is more sensible as we increase the working volume. We think that 200 µL is the ideal volume to work with this sensor, on the one hand, because of the results obtained and, on the other, because with larger volumes it runs the risk of overflowing.

Now that we have the results with the smaller sensor, we proceed to compare them with those obtained previously with Sensor 4. First, we will compare the results obtained with solution 1, 500 µL for Sensor 4 and 200 µL for Sensor 5.

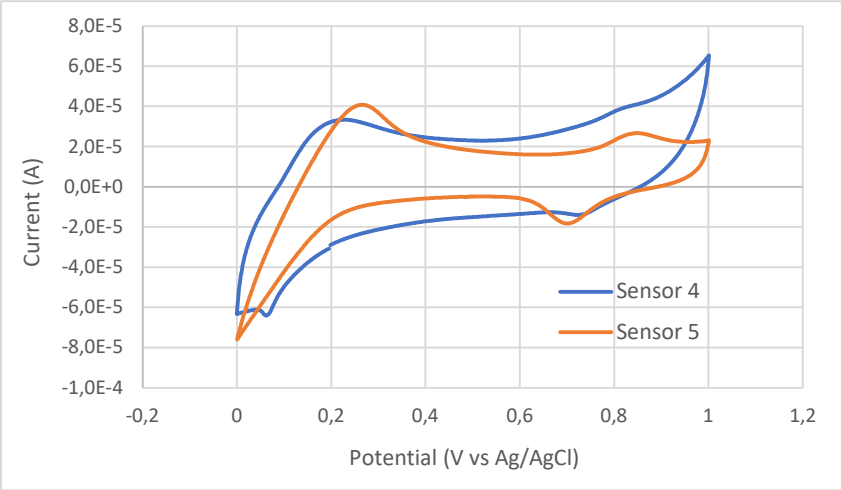

Figure 3.13. Comparation of cyclic voltammetry of Sensor 5 and Sensor 4 recorded at 0.05 V s^{-1} in 1 mM $K_3Fe(CN)_6$ and 0.1 M KCl (solution 1).

In the results we can see how the measurement with Sensor 4 has a greater signal, but that the one obtained with Sensor 5 presents the peaks with greater clarity. In both we can distinguish the anodic peak above 0.2 V that could belong to the species studied, although only in the measurement with Sensor 4 we can see the small signal in the cathodic area above 0.1 V. As for the peaks between 0.6 V and 0.8 V, they are more clearly visible in the result of the smaller sensor.

In view of the better performance of Sensor 5 for the same solution, we will compare the same results as above with those obtained with Sensor 4 when working with a more concentrated solution. Therefore, we compare the result of the measurement of 200 µL of solution 1 with Sensor 5 versus the measurement of 500 µL of solution 1 plus 100 µL of solution 2 with Sensor 4.

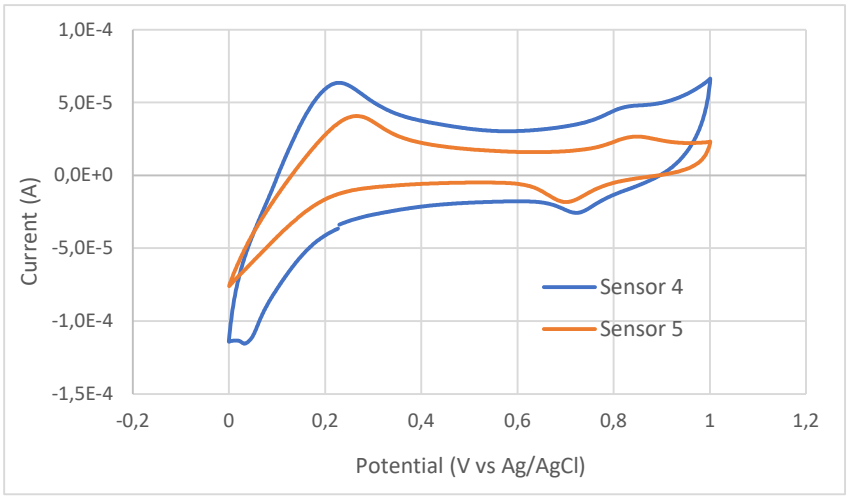

Figure 3.14. Comparation of cyclic voltammetry of Sensor 5 recorded at 0.05 V s^{-1} in 1 mM $K_3Fe(CN)_6$ and 0.1 M KCl (solution 1) and Sensor 4 recorded at 0.05 V s^{-1}in 1 mM $K_3Fe(CN)_6$ and 0.1 M KCl (solution 1) + 10 mM of $K_3Fe(CN)_6$ (solution 2).

The result obtained is very similar to the previous one. Comparing the voltammograms, we see that Sensor 5 shows more defined current peaks. This is caused directly by the sensor

size. The smaller sensor has a smaller capacitor, which means less capacitive current. Reducing the capacitive current the faradaic peaks are easily shown. Also, the sensor reduction influence on reaching faster the diffusion limit which also can be seen in higher intensity peaks corresponding to the non-complexed iron.

With all these results, we can conclude that the smaller the sensor size, the better the results. Not only that, but it also allows working with smaller volumes of solution and obtains better results with lower concentrations. For these reasons, together with the fact that less material is required to manufacture it, make it the best option, both in terms of results and sustainability. Also, we have to take into account the factor of its manufacturing difficulty, which is why once all the characteristics of the sensor have been analysed, we will conclude whether this option is the most efficient for the work we are carrying out.

3.1.3. Type of stencil used to paint the electrodes:

The electrodes of our sensors have been printed on paper with a brush and a stencil. This template presents the shape of our three electrodes and delimits the space where the conductive ink runs through. During this work, we have used two types of stencils, paper stencils and stencils made from PLA (PolyLactic Acid), each of which has its advantages. The main advantage of paper stencils is their ease of manufacture, as only an inkjet printer is required. These were printed on Din A4 paper, and their shape was cut out with a cutter. The main disadvantage is their limited lifetime, as they deteriorate with use and the relief of the electrodes eventually loses its shape. Another disadvantage is that, due to the poor adhesion between the paper template and the filter paper, the ink easily seeps under the template, so the relief of the working electrode had to be modified and made smaller, otherwise, there was a danger that it would come into contact with the auxiliary electrode. All the measurements that have been presented so far have been with sensors made with paper templates. On the other hand, we have those made from PLA (PolyLactic Acid) which are manufactured using a 3D printer. The main advantage of this type of template is its rigidity, which allows to paint of more defined and wider electrodes, as well as a larger working electrode, which should lead to better results. Their greater rigidity also translates into greater strength and therefore means that these stencils have a longer useful life. The main drawback is the difficulty in manufacturing them, as a 3D printer is required.

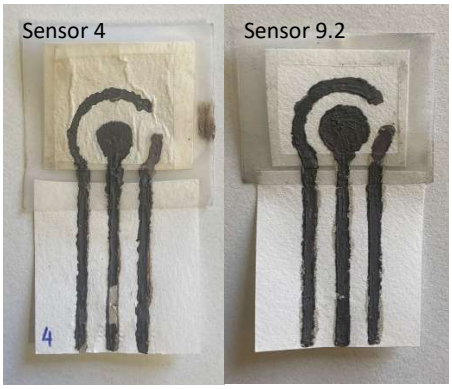

Figure 3.15. Comparation between Sensor 4 (paper stencil) with Sensor 9.2 (PLA stencil).

To study which of the two different types of masks gives the best results, we will analyse the measurements on different solutions. For solutions 1 and 2, we will compare the results obtained with Sensor 9.2 (manufactured with PLA stencil) with those obtained with Sensors 4 and 5 (manufactured with paper stencil). We will also make measurements on a solution of 0.02 M $CuSO_4$ and 0.1 M H_2SO_4 which we will refer to from now on as solution 3. For this analyte, we will compare the results obtained with Sensors 4 and 6 (paper) with those obtained with Sensor 9.2 (PLA).

We start by analysing the results of Sensor 9.2 with solutions 1 and 2. The setup is the same as before, a three-electrode setup, and we start by studying 500 µL of solution 1. The results are shown in Figure 3.16.

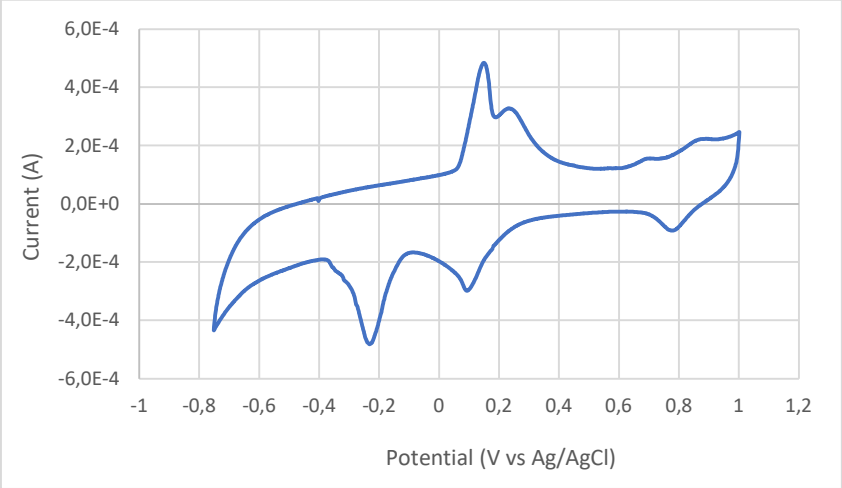

Figure 3.16. Cyclic voltammetry of Sensor 9.2 recorded at 0.05 V s^{-1} in 1 mM $K_3Fe(CN)_6$ and 0.1 M KCl (solution 1).

At a first glance, the appearance of some peaks that we had not observed until now is already noticeable. In this voltammogram, we can see 4 peaks in the anodic scan, two of higher intensity between 0.15 and 0.3 V and two wider, one at 0.7 and the other at 0.9 V. In the anodic scan, we see three more peaks at -0.2, 0.1, and 0.8 V. Centred on the 0 V potential we see the two peaks at -0.2 V and 0.2 V. These two peaks would correspond to an interference caused by a reaction at the reference electrode. As we have explained before in the sensor fabrication section, in case part of the first silver layer of the electrodes reaches the working area, and in the presence of chloride ions, the reaction $Ag + Cl^- \rightarrow AgCl + e^-$ may occur, as well described and exemplified in the literature[7]. The two peaks at 0.1 and 0.2V are attributed to the $K_3Fe(CN)_6$ and the two at 0.8 and 0.9 V to the non-complexed iron.

Now that we can finally observe the two signals belonging to our analyte, we proceed to try to isolate them so that the interference caused by the oxidation of the silver is left out of our measurement. This is why we perform a scan with the same volume and solution but reducing the minimum potential to -0.1 V.

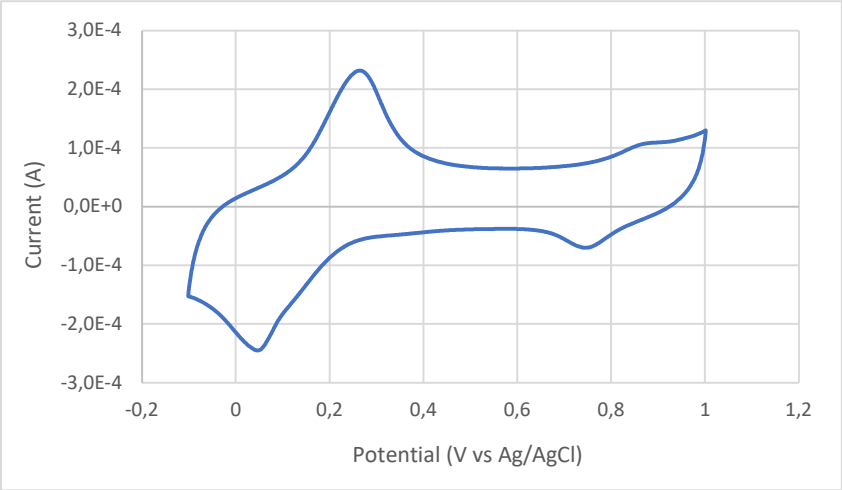

Figure 3.17. Cyclic voltammetry of Sensor 9.2 recorded at 0.05 V s^{-1} in 1 mM $K_3Fe(CN)_6$ and 0.1 M KCl (solution 1).

In this result, we no longer see the interference of silver. Compared to the previous measurement we can see that all the peaks have been shifted to lower potentials. Even so, we can still see the two iron peaks at high potentials and the two peaks due to $K_3Fe(CN)_6$. Once we have been able to isolate our interference measurement, we study the effect of the analyte concentration. We will therefore compare the latter result with two more scans, one with 300µL of solution 1 and 100 µL of solution 2, and the other with 300 µL of solution 1 and 200 µL of solution 2.

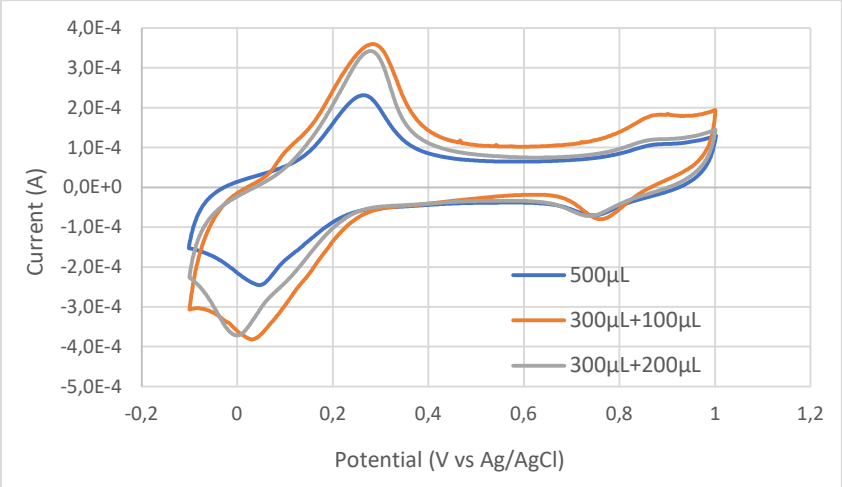

Figure 3.18. Comparation of cyclic voltammetry of Sensor 9.2 with 500 µL of solution 1, 300 µL of solution 1 + 100 µL of solution 2 and 300 µL of solution 1 + 200 µL of solution 2.

The result is as expected, as we can see that as the concentration increases, the intensity of the peak signal also increases. We can also see that, at higher concentrations, the peaks tend to shift to lower potentials.

With the results obtained from Sensor 9.2, we proceed to compare them with those obtained previously for Sensors 4 and 5.

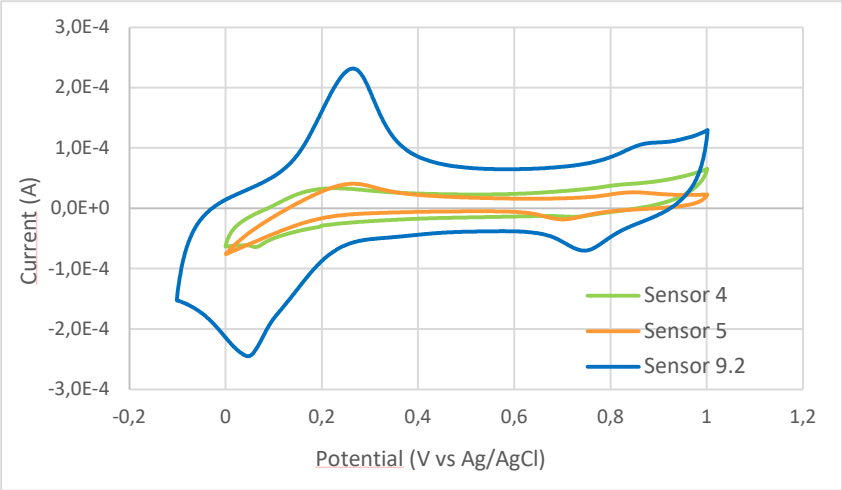

Figure 3.19. Comparation between cyclic voltammetry of Sensor 4, Sensor 5 and Sensor 9.2 recorded at 0.05 V s^{-1} in 1 mM $K_3Fe(CN)_6$ and 0.1 M KCl (solution 1).

As can be seen, the results for Sensor 9.2 are more satisfactory. The signals for all peaks are much larger and more defined, as well as showing signals that are not even noticeable in the other measurements. However, we have previously seen the possibility that the signals corresponding to the analyte are shifted to more negative potentials than expected. This is why we could think that in the analyses carried out with Sensors 4 and 5 for the same solution, we might not have perceived the signals of the peaks of interest, since in these the minimum potential for the lowest scanning range has always been 0 V. Likewise, it is also true that in reducing the minimum potential the result is more susceptible to be affected by the interference of the reaction of the reference electrode, and in view of the lower sensitivity of these last two named devices, the result would be even more affected by this interference. Also, we can see that although the capacitive current for Sensor 9.2 is way higher than for the other sensors, the peaks are well distinguished, which is another proof of this sensor's better sensitivity.

After studying the results with this solution, we will compare the measurements taken with solution 3. First, we will look at the results of the sensors made with a paper template, Sensor 4, and Sensor 6.

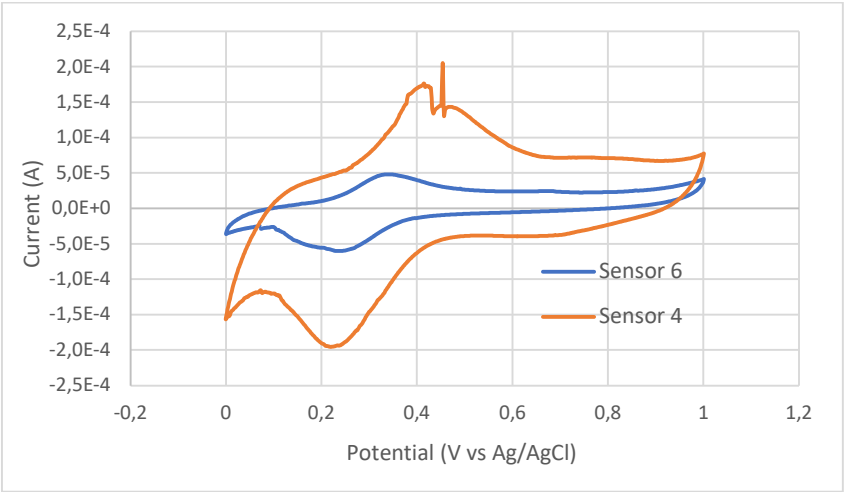

Figure 3.20. Comparation of cyclic voltammetry of Sensor 4 and Sensor 6 recorded at 0.05 V s^{-1} in 20 mM $CuSO_4$ and 0.1M H_2SO_4 (solution 3).

Both sensors give good results, as they show two signals in the potential region where we would expect to find those of the analyte. In the anodic scan we can see a peak at 0,3 V for Sensor 6 and at 0.4 V for Sensor 4, while in the cathodic scan both sensors show a current peak at 0.25 V.

We now look at the results with Sensor 9.2. In this scan the minimum potential is reduced to -0.65 V since we did not observe any peaks of interest at the same scan range used for Sensors 4 and 6.

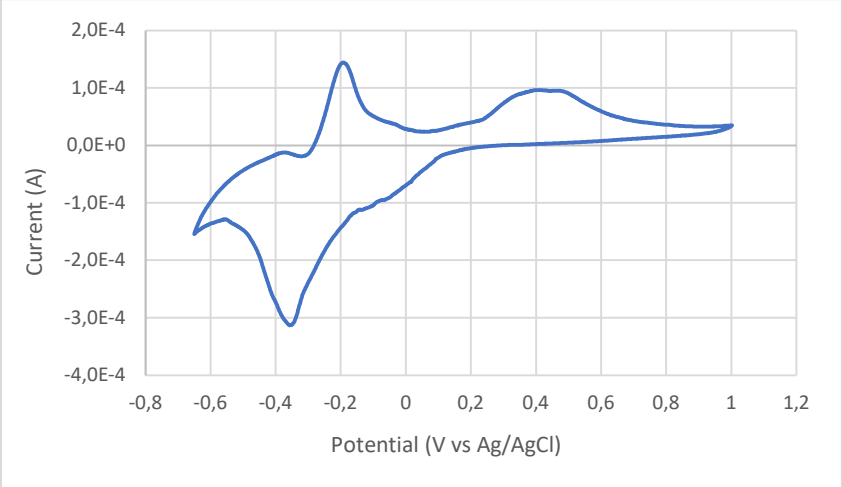

Figure 3.21. Cyclic voltammetry of Sensor 9.2 recorded at 0.05 V s^{-1} in 20 mM $CuSO_4$ and 0.1M H_2SO_4 (solution 3).

In this voltammogram, we observe three peaks in the anodic scan at -0.4, -0.2 and one low and broad at 0.4 V, and one more in the cathodic scan at -0.35 V. The pair of peaks at -0.35 and -0.2 V could be attributed to the reversible redox characteristics of $CuSO_4$ since is the only redox behaviour observed in the scan. In that case, would that mean that both peaks have been displaced to more negative potentials. To determine this with certainty, we study the anodic peaks. We performed three linear sweep voltammetries, one with solution 3 alone, the next one by adding a drop of KCl, and the last one by adding a drop of a copper complex with neocuproine.

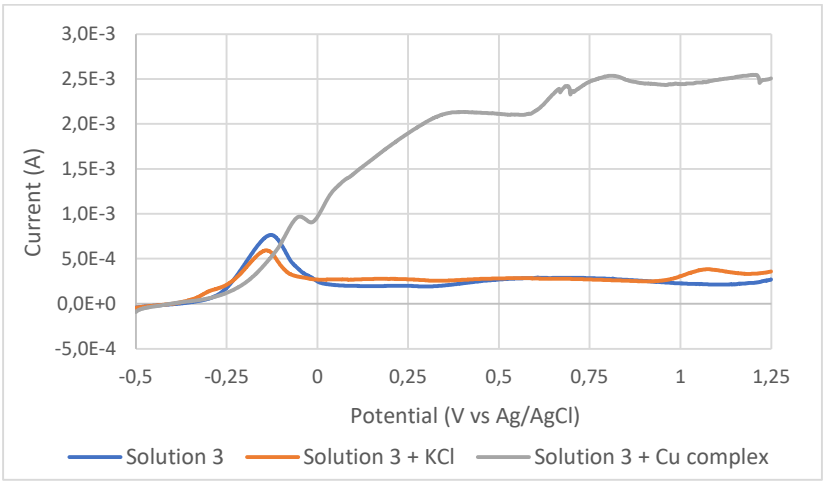

Figure 3.22. Comparation of linear sweep voltammetry of 20 mM $CuSO_4$ and 0.1M H_2SO_4 (solution 3).

We can see that when the KCl solution is added, the first peak decreases, probably because the concentration of the analyte is reduced. On the other hand, when adding the

solution with the copper complex, we can see how the first peak shifts, so we can attribute the first peak to the $CuSO_4$ signal. Now that we have all the results with solution 3, we can compare them with each other.

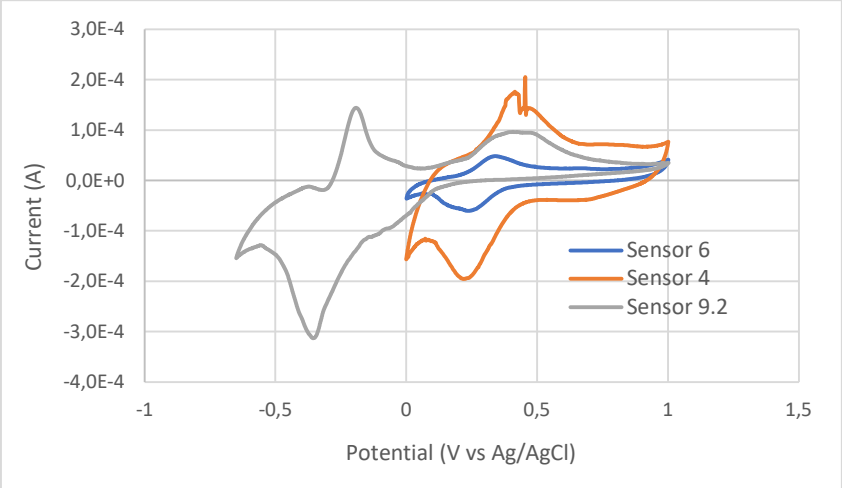

Figure 3.23. Comparation of cyclic voltammetry of Sensor 9.2, Sensor 4 and Sensor 6 recorded at 0.05 V s^{-1} in 20 mM $CuSO_4$ and 0.1M H_2SO_4 (solution 3).

The first thing we can see is the potential difference where the interest signals appear, and that the three sensors share an anode peak at 0.4V. What is noticeable is the better performance of Sensors 4 and 9.2 compared to Sensor 6, as they show results with a higher signal.

Having all the results, we will decide on a type of template for the sensors. In the studies on solutions 1 and 2, there is a clear better performance of Sensor 9.2. It clearly shows the peaks of interest with much higher signals. As for the study on solution 3, we have very similar results with Sensor 4 and Sensor 9.2. To try to clarify which of the two is better we can compare their results over a larger scanning rate of 0.1 V s^{-1}.

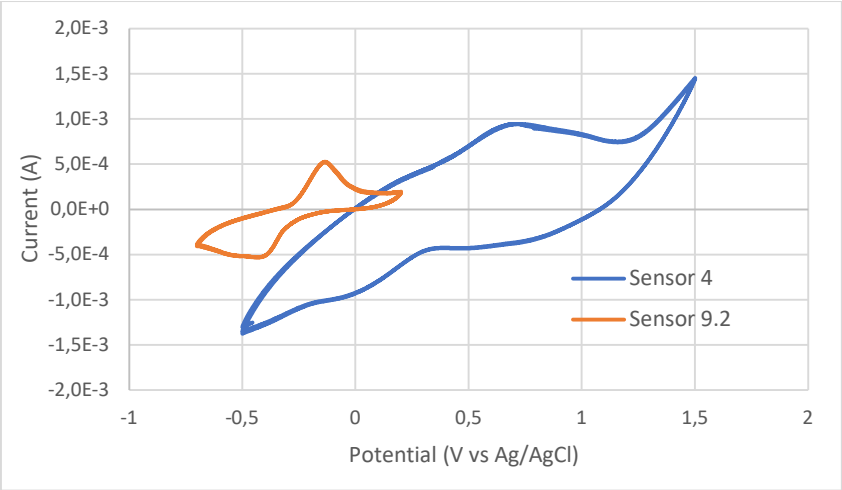

Figure 3.24. Comparation of cyclic voltammetry of Sensor 9.2 and Sensor 4 recorded at 0.1 V s^{-1} in 20 mM $CuSO_4$ and 0.1M H_2SO_4 (solution 3).

At a larger scanning rate, the faradaic peaks are more difficult to be shown, so as we can see Sensor 9.2 presents more sensibility as is capable of recognising the studied signals.

Given the good performance of solutions 1 and 2, and although the results for solution 3 are somewhat ambiguous, we opted for the PLA (PolyLactic Acid) stencil manufactured with a 3D printer, as it offers more sensitive and more durable electrodes.

3.2 HUMIDITY SENSING

To explore the possibilities offered by our device, we performed a humidity test. This test does not require the immersion of the sensor or the deposit of any substance on its surface. To assess relative humidity, we performed measurements at different humidities in a controlled environment.

To carry out this procedure, we employed a container, in our case a desiccator, where we introduced a solution of water with $CaCl_2$. $CaCl_2$ is a substance with hygroscopic properties, i.e. it tends to absorb the water found in the environment. $CaCl_2$ is also an electrolyte very soluble in water, and by controlling its concentration, we can know the relative humidity level inside our container, as reported in Table 3.1.

Table 3.1. Relative humidity obtained in an atmosphere equilibrated with a solution of $CaCl_2$ at a given concentration.

Relative humidity %	$CaCl_2$ weight %
90	14.95
80	22.25
70	24.95
65	29.64
60	31.73
50	35.64
40	39.62
30	44.36

By performing chronoamperometries we will expect to see an increase in the electric current as we increase the ambient humidity, because the water content inside the paper, a porous medium, will increase (increasing the ionic mobility), and therefore its resistivity will drop significantly. Therefore, we expect that the average current once it has stabilised will increase, increasing relative humidity. For this setup we will use sensor number 9, i.e., a sensor with two-layer electrodes (silver ink and graphite) painted with a paper stencil, and for the chronoamperometry we will only use the working and auxiliary electrodes in a two-electrode cell setup (Figure 3.25).

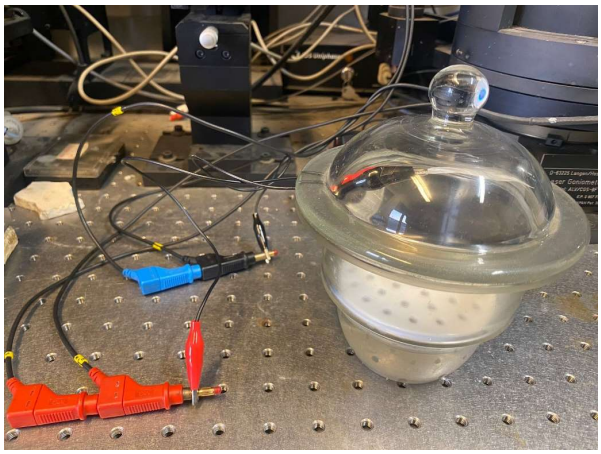

Figure 3.25. Setup employed for relative humidity sensing. The sensor is located in the desiccator headspace, equilibrated with a $CaCl_2$ solution. The connections of working and auxiliary electrode are visible in the two-electrode setup.

The average values obtained for each RH% are shown in Table 3.2 and the results of the chronoamperometries at different RH% are shown in Figure 3.26.

Table 3.2. Average current values of the chronoamperometries at different RH%.

Relative humidity (%)	Average stabilised current (A)
30	6.33E-10
40	5.80E-9
50	9.37E-9
60	1.62E-8
70	2.72E-8
80	4.53E-8
90	8.72E-8

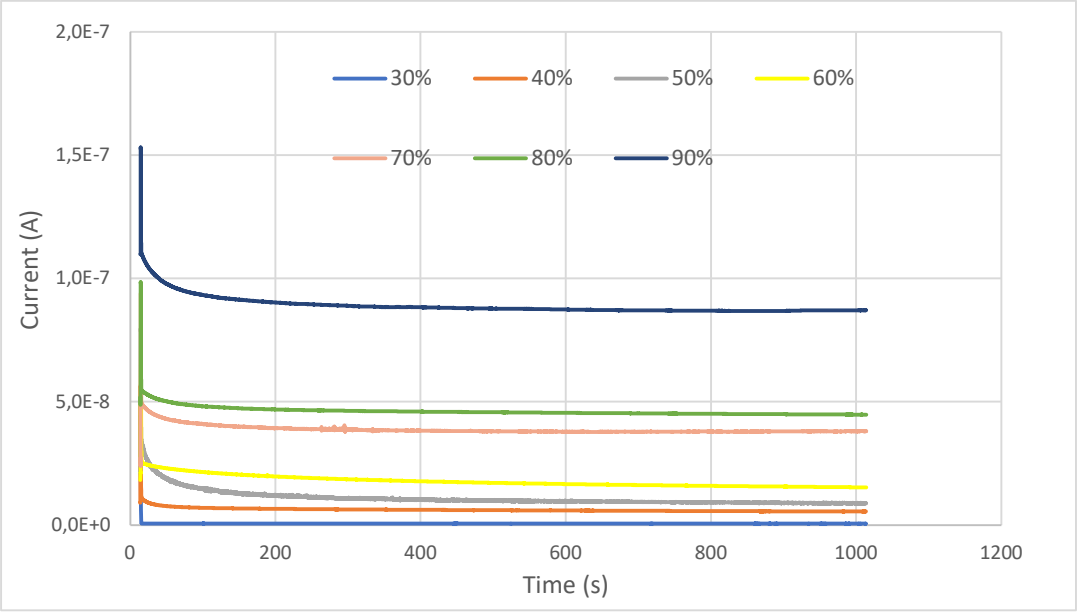

Figure 3.26. Chronoamperometries at different RH% value.

As we can see in the results, we obtained the expected behaviour as the electric current increased with the RH% value. With the average current values obtained, we build a calibration curve of current vs relative humidity %. Figure 3.27 reports this calibration curve. The curve is exponential with equation $y=1.795E\text{-}10e^{0.0713x}$ and $R^2 = 0.9934$.

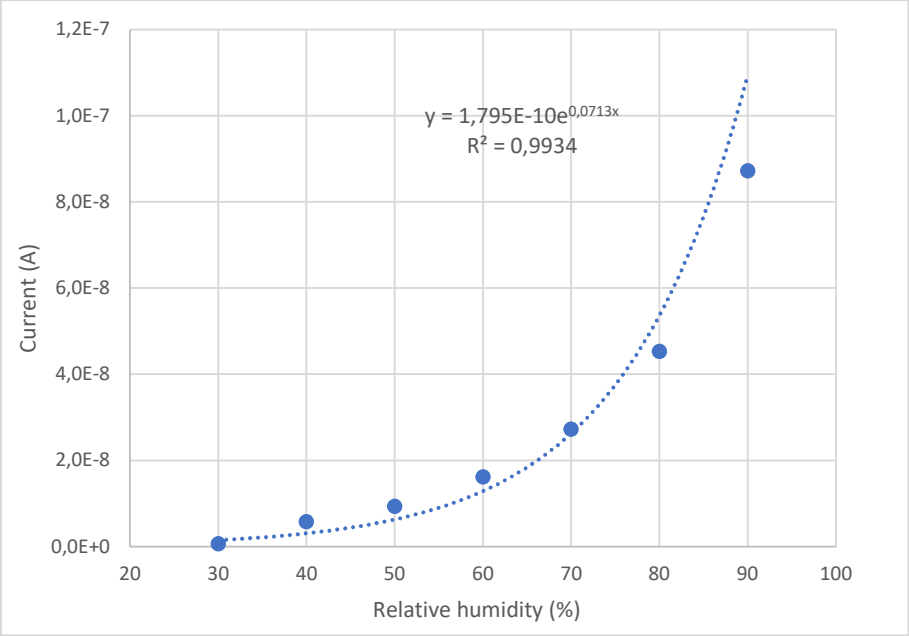

Figure 3.27. Calibration curve of average current values vs %RH.

To test the capability of this curve to recognise the values used to build the regression curve we are going to study the recovery values. These values are obtained by comparing the nominal values obtained by experimentation with the ones that are obtained using the regression curve for the same RH% value.

Table 3.3. Recovery calculated as the ratio between RH calculated with the regression curve of Figure 3.27 and nominal RH.

Relative humidity %	Current (A)	Relative humidity % found with regression	Recovery %
90	8.72E-8	86.75	96.38
80	4.53E-8	77.57	96.96
70	2.72E-8	70.44	100.63
60	1.62E-8	63.15	105.25
50	9.37E-9	55.47	110.94
40	5.80E-9	48.74	121.85
30	6.33E-10	17.67	58.90

A more rigorous procedure would be calculating the humidity value excluding that sample from the regression to obtain a new recovery value, in order to test the prediction ability of the curve. This time computed values are obtained through a regression equation obtained with 8 relative humidity values only, and without the value under consideration. Recovery values

were obtained by comparing the values found through regression with nominal values and are sown in Table 3.4.

Table 3.4. Recovery calculated as the ratio between RH calculated with the regression curve obtained without the value under consideration and nominal RH.

Relative humidity %	Regression equation	Relative humidity % found with regression	Recovery %
90	$y=1.4E\text{-}10e^{0.0758x}$	84.15	93.50
80	$y=1.7E\text{-}10e^{0.0729x}$	76.69	95.87
70	$y=1.8E\text{-}10e^{0.0711x}$	70.60	100.85
60	$y=1.7E\text{-}10e^{0.0712x}$	63.67	106.13
50	$y=1.5E\text{-}10e^{0.0729x}$	56.59	113.18
40	$y=1.1E\text{-}10e^{0.0775x}$	51.28	128.22
30	$y=6.5E\text{-}10e^{0.0537x}$	-0.50	-1.68

Most of the results of this recovery are more deviated from the 100% compared with the values obtained with the first recovery. The reason for this situation is that the samples this time are totally unknown to the model. Also, we can observe that the recovery value for the 30% shows a big deviation, this is due to this value being calculated by extrapolation, whereas from 40-80% the values are calculated by interpolation. 90% value is calculated by extrapolation as well, but in this case, the curve shows a better prediction ability.

3.3. LIGHT INCIDENCE SENSING

One possibility offered by the sensors we are working on is to modify their characteristics to make them sensitive to different analytes and physical properties. There are two main types of modifications, those that are applied to the working area of the sensor and absorbed by the filter paper, and those that are applied to the working electrode, either on its surface or mixed with the ink we use to paint the electrodes.

In our case, we are going to test the second of these possibilities. Our intention is to test the photocatalytic properties of TiO_2 and to see if the design and configuration of our sensor can distinguish between periods of incidence and non-incidence of light at different light intensities. For this purpose, we have made different modifications to our sensor, where we highlight two different types. One type of modification consists of spreading a liquid compound with TiO_2 over the working area of our sensor. The liquid compound in one case consists of TiO_2 and water, and the sensors to which we have applied it are number 7 and number 13. In the other case, the compound consists of TiO_2 and a mixture of nail polish and acetone. It should also be noted that the electrodes of Sensor 13 are only painted with silver ink. The other type of modification consists of adding the TiO_2 to the ink with which we paint the working electrode, and the sensors where we have applied this method are 11, 10 and 12 with concentrations of 2%, 10% and 50% of TiO_2 in the ink respectively.

Table 3.5. Type of modification, sensor number and modification specifications.

Type of modification	Sensor number and modification		
On the WE surface	Sensor 7: water + TiO_2	Sensor 13: water + TiO_2; silver electrodes	Sensor 8: nail polish + acetone + TiO_2
In the ink of the WE	Sensor 11: 2% TiO_2 in the ink	Sensor 10: 10% TiO_2 in the ink	Sensor 12: 50% TiO_2 in the ink

When TiO_2 is irradiated with visible light of energy equal to or higher than the energy of the forbidden band, the electrons of its valence band are excited to its conduction band, leaving holes in the first band mentioned. This results in an increase in the electric current and a decrease in the potential in the sensor, which can be quantified by chronoamperometry and chronopotentiometry.

For this experiment, we will use a three-electrode setup and a spotlight. Our sensor will be arranged vertically with the working electrode facing the spotlight, and its working area will be wetted either with a solution of 0.1 M KCl or 0.1M KNO_3. To regulate the light intensity, measurements will be taken at different distances from the source of irradiation and to control the periods of light and darkness, a lid covered with aluminium foil will be used.

To establish which sensor performs better, we will analyse the results of all sensors and then compare the results of each type (TiO_2 on WE or TiO_2 in the ink) with each other. Finally, we will compare the results between the two types. In addition, in some cases, we will also compare the sensor designs (Design 1 and Design 2) and see if they are decisive for the results.

3.3.1. Potentiometric measurements:

We started our experience by performing chronopotentiometry on our sensors and the first one to be tested is the Sensor 7.

Table 3.6. Incidence and non-incidence of light periods and light irradiance intensity.

No light incidence periods (s)	Light incidence periods (s)	W m^{-2}
0-56	56-200	0.65
200-350	350-600	1.80
600-1000	1000-1100	
1100-1170	1170-1600	25.63
-	1600-1700	181.55

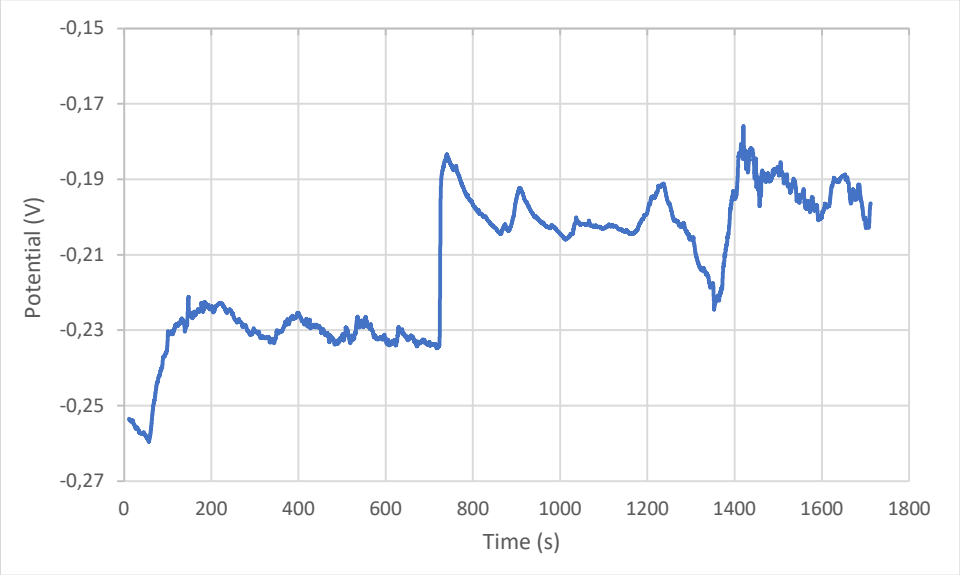

Figure 3.28. Chronopotentiometry of Sensor 7 in 0.1 M KCl.

At 730 seconds of the measure, we added 100 µL of the KCl solution. At the beginning of the analysis, the sensor has some response to the light incidence, since we can observe that there are two peaks at 56 seconds and at 200 seconds, coinciding with the dark/light periods. Even so, as we can observe, the behaviour is the opposite as we were expecting (the potential is decreasing in the dark period and increases during irradiation). At 400 seconds the sensor stops responding to light incidence. We supposed that this is because the solution has dried up, so we added 100 µL of electrolyte. From that moment the measurement demonstrated minor potential changes upon irradiation variations, but the trend is very noisy, and some features cannot be correlated with varying irradiation conditions.

With the same setup and procedure, we carry out the measurement on Sensor 8.

Table 3.7. Incidence and non-incidence of light periods and light irradiance intensity.

No light incidence periods (s)	Light incidence periods (s)	W m^{-2}
0-50	50-130	0.65
130-160	160-300	1.80

300-340	340-400	25.63

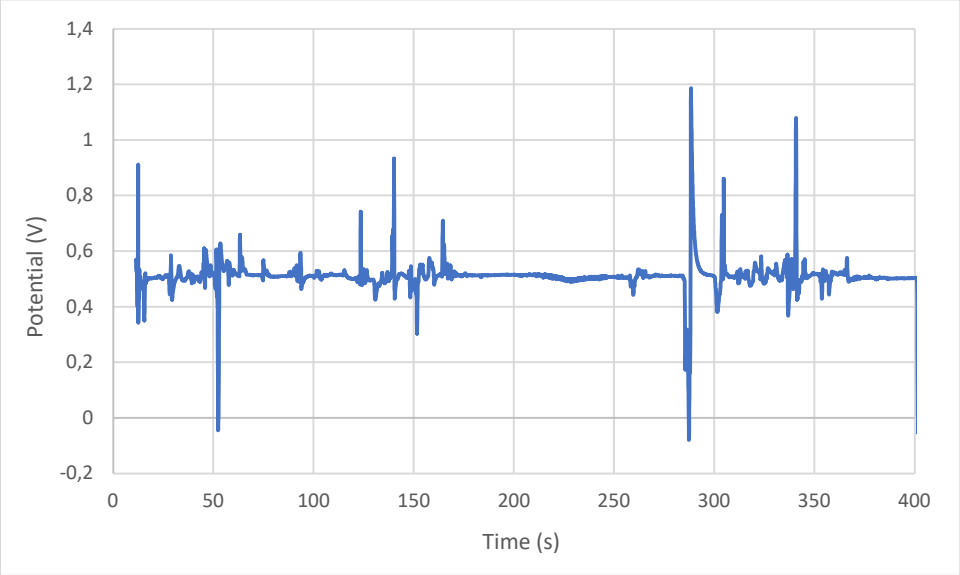

Figure 3.29. Chronopotentiometry of Sensor 8 in 0.1 M KCl.

As we can see, the sensor never responds to the incidence of light, which suggests that the mixture of acetone and nail polish does not allow conductivity between the TiO_2 and the working electrode. In this measurement we again observe that the solution that wets the working area dries easily.

Since applying a small volume of electrolyte to the working area is a disadvantage, we are making a change in the installation. In order to prevent this solution from drying out, from now on all measurements are made with the sensor immersed in the electrolyte so that the installation is as follows:

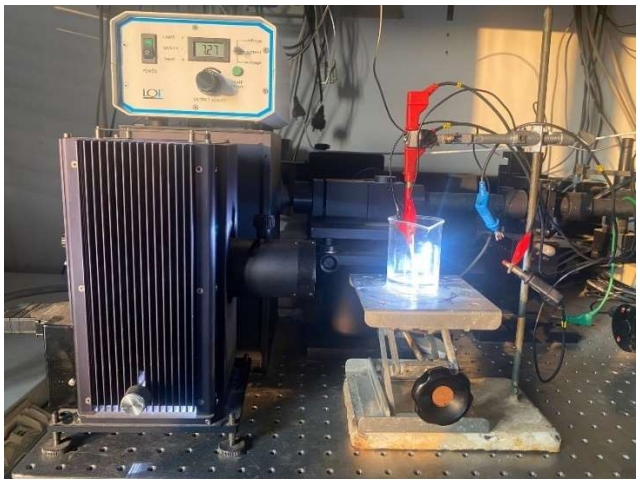

Figure 3.30. Setup employed for light sensing. The sensor is located vertically, with the working area centered in the spotlight.

With the new set-up, the measurement is again carried out on Sensor 7.

Table 3.8. Incidence and non-incidence of light periods and light irradiance intensity.

No light incidence periods (s)	Light incidence periods (s)	W m^{-2}
0-90	90-140	0.65
140-420	420-600	1.80
600-1500	1500-1640	25.63
1640-2020	2020-2480	181.55
2480-2730	2730-3000	

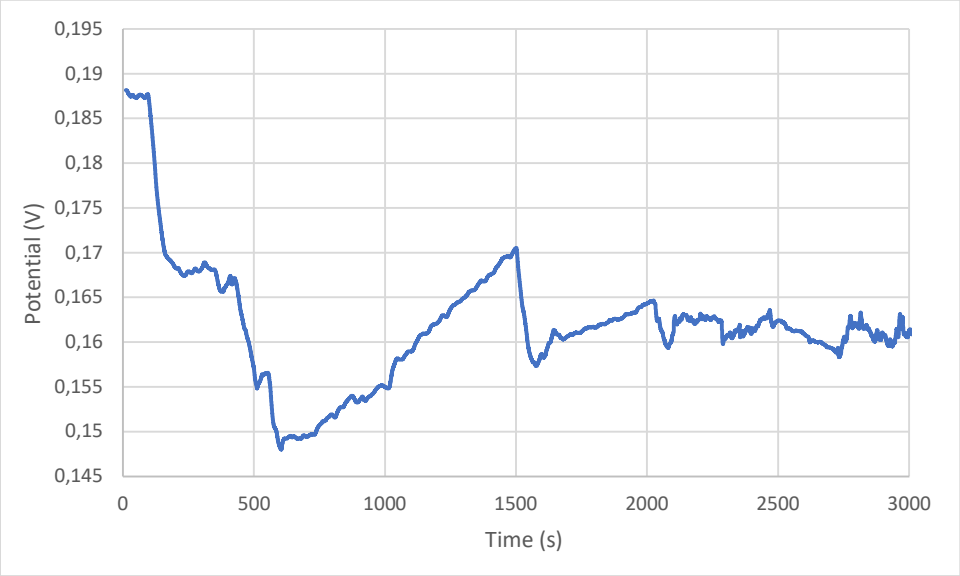

Figure 3.40. Chronopotentiometry of Sensor 7 in 0.1 M KCl.

With the sensor immersed, we don't have de drying out problem anymore. The device responds to the light incidence as we were expecting (the potential is going down in the light incidence periods and going up when the sensor is covered and not reached by the light). In the beginning, we can observe that the reaction of the light incidence is less noticeable, the measurement shows the changes between the light and dark periods, but even so, the peaks are not relevant enough. Then from the second 420 to 1500, the peaks are sharper, and the sensor response is quicker. From 1500 seconds the sensor stops showing a response to any known stimulus.

We made one more measurement with Sensor 7 but did not obtain any satisfactory results, so we moved on to the next sensor, Sensor 10, which is the first representative of those with a modification in the ink of its WE.

Table 3.9. Incidence and non-incidence of light periods and light irradiance intensity.

No light incidence periods (s)	Light incidence periods (s)	W m^{-2}
0-90	90-160	0.65
160-260	260-460	1.80

460-660	660-940	25.63
940-1240	1240-1500	
1500-1900	1900-2000	
2000-2300	2300-2700	
2700-3000	-	

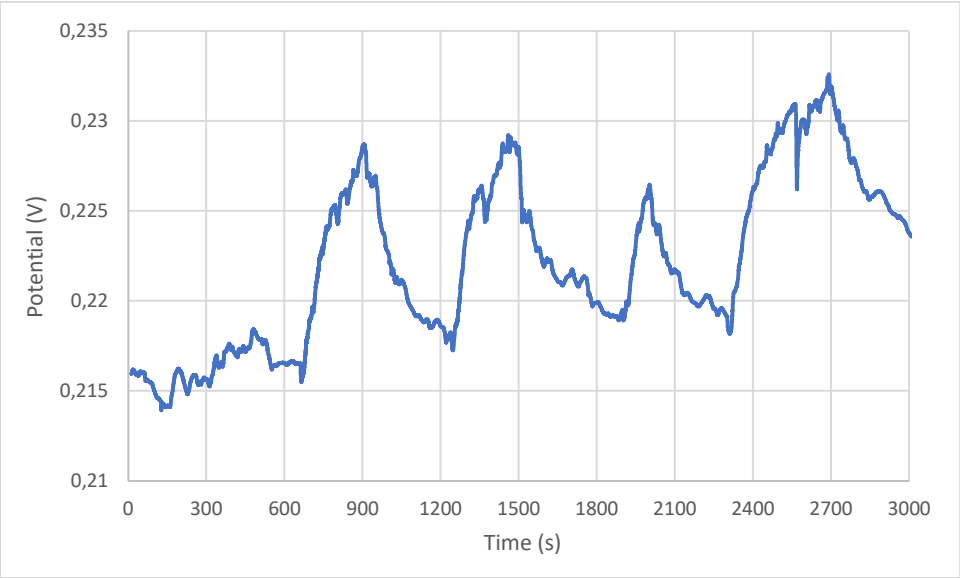

Figure 3.41. Chronopotentiometry of Sensor 10 in 0.1 M KCl.

At 660, when we approach the sensor 10 cm from the light, it starts working. From then on, the measurement shows the best signal and quickest response to the incidence of light until that moment. But the particularity of this measurement is that the response is the opposite of the one that we were expecting, seeing an increase of the potential when the device is exposed to light and a decrease when it is out of the spotlight.

Given this strange behaviour, we repeated the measurement with this sensor. Seeing that it worked well from the moment it was working with a light incidence of 25.63 W m^{-2}, we carried out the whole procedure at the same intensity.

Table 3.10. Incidence and non-incidence of light periods and light irradiance intensity.

No light incidence periods (s)	Light incidence periods (s)
0-100	100-300
300-600	600-900
900-1200	1200-1300
1300-1400	1400-1500
1500-2000	2000-2400
2400-2600	2600-2700
2700-3000	-

Figure 3.42. Chronopotentiometry of Sensor 10 in 0.1 M KCl.

The sensor starts responding to the incidence of light 600 seconds approximately from the beginning of the valuation. As we can observe it recovered its normal behaviour (potential increase during excitation and decrease during relaxation). For the first time, we can see in some cases (900-1200 seconds; 1500-2000 seconds; 2400-2700 seconds) that when the potential is increasing, it tends to stabilize at some point instead of continuing increasing.

At this point we are starting to see the first satisfactory results and since we have now verified that Sensor 10 can perform as expected, we have come up with a modification to find a middle ground between the two different types of sensors we are analysing. Therefore, we apply a layer of the TiO_2 solution in water (the same as in Sensors 7 and 13) on the working electrode of Sensor 10 and proceed to carry out the relevant measurements. As in the previous analysis, the intensity of the focus will be 25.63 W m^{-2} during the whole procedure.

Table 3.11. Incidence and non-incidence of light periods and light irradiance intensity.

No light incidence periods (s)	Light incidence periods (s)
0-90	90-190
190-400	400-600
600-900	900-1100
1100-1300	1300-1500
1500-1600	1600-1700
1700-2100	2100-2180
2180-2300	2300-2700
2700-2900	2900-3000

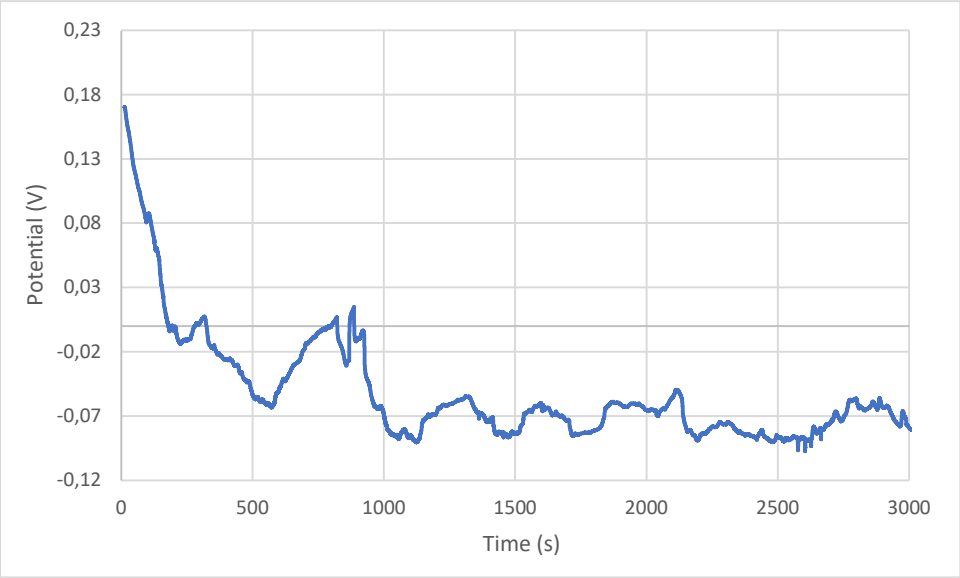

Figure 3.43. Chronopotentiometry of Sensor 10 in 0.1 M KCl.

The sensor starts working between 400-600 seconds from the start of the measurement. Despite that it responds to light, the signal is very low as in the last measurement. We can also observe the same stabilization behaviour when the potential is increasing in some of the peaks.

We performed some more short-term measurements. We observed better results when starting the analysis with the sensor under the incidence of light. For this reason, we performed a more long-term analysis on this modified device, starting the measurement with the sensor under the spotlight of the lamp. Now the light intensity will be 38.40 W m^{-2} during the whole measurement.

Table 3.12. Incidence and non-incidence of light periods and light irradiance intensity.

No light incidence periods (s)	Light incidence periods (s)
-	0-100
100-300	300-400
400-500	500-600
600-800	800-900
900-1100	1100-1150
1150-1350	1350-1450
1450-1650	1650-1750
1750-1950	1950-2050
2050-2250	2250-2350
2350-2550	2550-2650
2650-2850	2850-2950

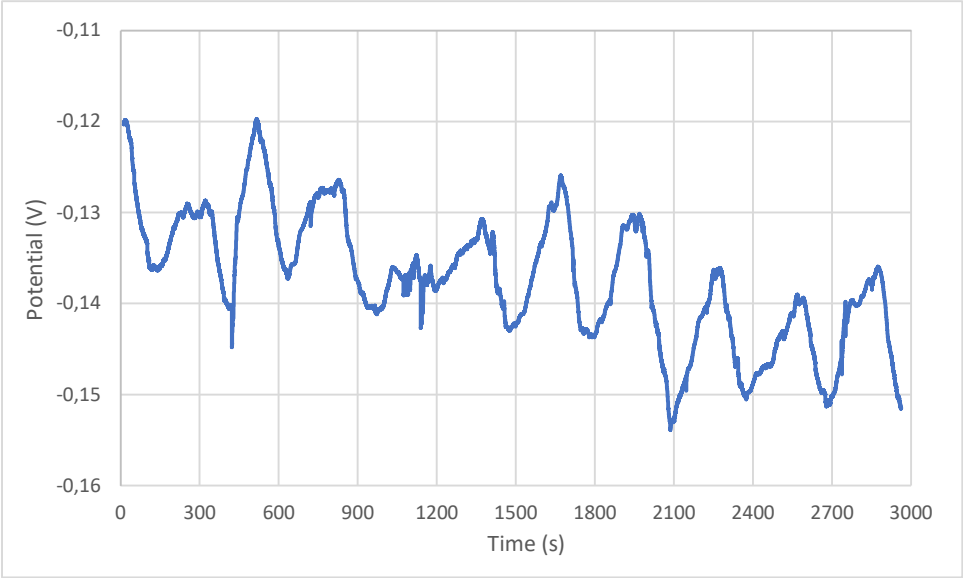

Figure 3.44. Chronopotentiometry of Sensor 10 in 0.1 M KCl.

Seeing that the sensor response is better when the measurement starts with light incidence, all the measurements from now on are carried out this way. The result obtained is the one expected, with a quick response and sharp peaks. With the information obtained in the last evaluation, we are trying to know which are the optimal times for both, light and dark periods, to acquire the clearest signals. As we observe in the previous measurements, if we let the sensor excite or relax for too long, it tends to stabilise the potential, and the noise became more notable. So, to avoid these plateaus, we are limiting the excitation (light period) to just 100 seconds, and the dark periods to the double of time, due to the relaxation is slower. In order to try if this period could be reduced, we tried to do a light period of 50 seconds (1100-1150 seconds), but it resulted in a noisy and blurred signal.

Continuing with the modified ink sensors, we now move on to chronopotentiometry with Sensor 11. Because the results we obtain are of short duration, we present them both together below. For both sensors, the light intensity during the whole process is 25.63 W m^{-2}.

Table 3.13. Incidence and non-incidence of light periods and light irradiance intensity.

No light incidence periods (s)	Light incidence periods (s)
0-100	100-300
300-400	400-600
600-700	700-800
800-900	900-1000

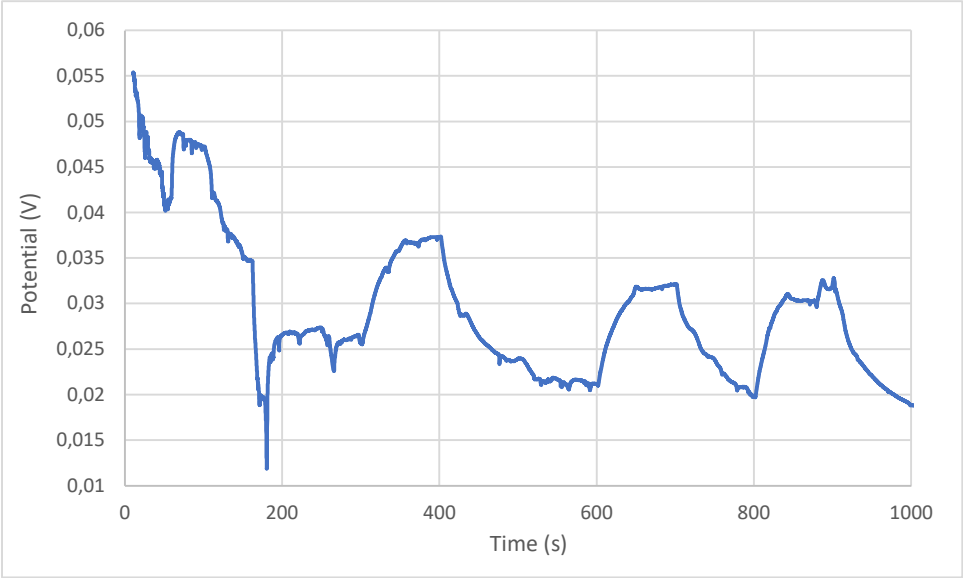

Figure 3.45. Chronopotentiometry of Sensor 11 in 0.1 M KCl.

Table 3.14. Incidence and non-incidence of light periods and light irradiance intensity.

No light incidence periods (s)	Light incidence periods (s)
-	0-100
100-200	200-300
300-400	400-500
500-600	600-700

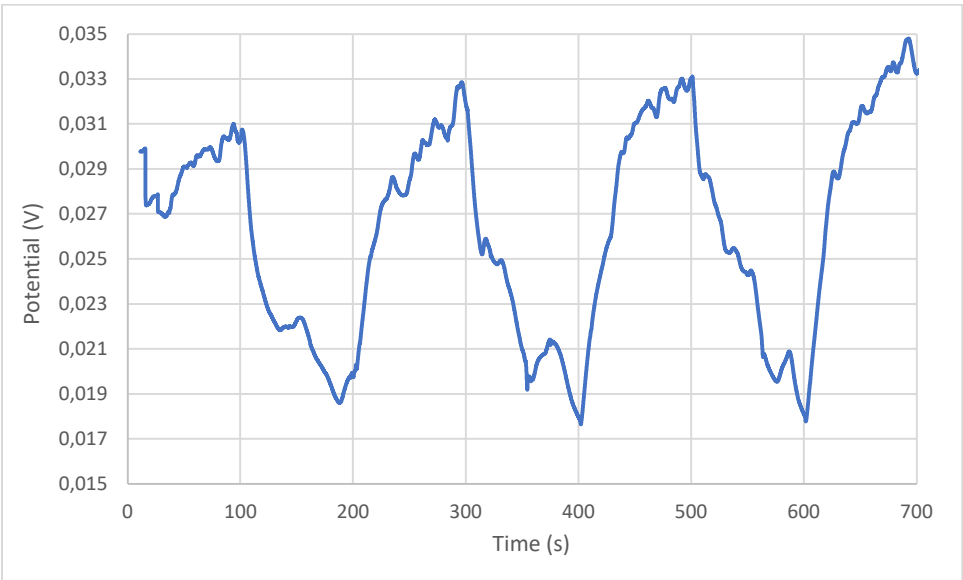

Figure 3.46. Chronopotentiometry of Sensor 11 in 0.1 M KCl.

In both measurements we observe the same behaviour, the response to the light incidence is fast and the peaks are clear. The main point in these two measurements is that again we see the opposite as we were expecting. The potential is going down during the light periods and going up during the dark.

To find an explanation for this phenomenon, we decided to first perform the analysis with the two remaining sensors, numbers 12 and 13, to see if they also behave in the same way. We start with the number 12. The light intensity for the whole procedure is 25.63 W m^{-2}.

Table 3.15. Incidence and non-incidence of light periods and light irradiance intensity.

No light incidence periods (s)	Light incidence periods (s)
-	0-100
100-300	300-400
400-600	600-700
700-900	900-1000
1000-1200	1200-1300
1300-1500	1500-1600
1600-1800	1800-1900
1900-2100	2100-2200
2200-2400	2400-2500
2500-2700	2700-2800
2800-3000	-

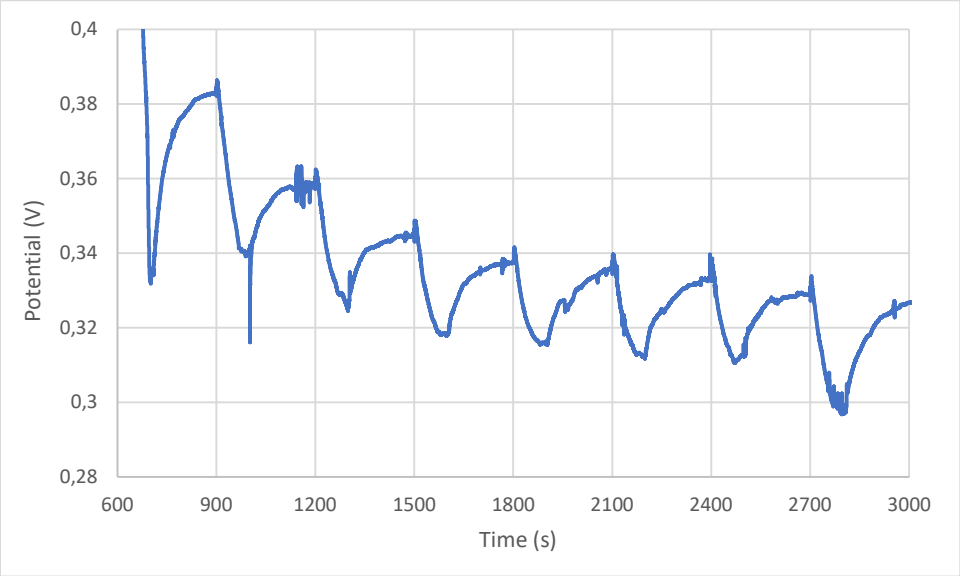

Figure 3.47. Chronopotentiometry of Sensor 12 in 0.1 M KCl.

This sensor behaves as we were expecting. It needs 600 seconds to start working properly, and because of that we only present the result from the second 600, but from then on, the response obtained is maybe the best for the moment. As we can see, the excitation and relaxation periods are well distinguished, the stabilisation of the potential observed at the top of the peaks is not very affected by the noise, and all the peaks have good reproducibility between them. Also, we can observe a tendency to a potential reduction from the first to the last peak.

Finally, we present the results of Sensor 13, also at 25.63 W m^{-2}.

Table 3.16. Incidence and non-incidence of light periods and light irradiance intensity.

No light incidence periods (s)	Light incidence periods (s)
-	0-100
100-200	200-300
300-400	400-500
500-600	600-700
700-800	800-900
900-1000	1000-1100
1100-1200	1200-1300
1300-1400	1400-1500
1500-1600	1600-1700
1700-1800	1800-1900
1900-2000	2000-2100
2100-2200	2200-2300
2300-2400	2400-2500
2500-2600	2600-2700
2700-2800	2800-2900
2900-3000	-

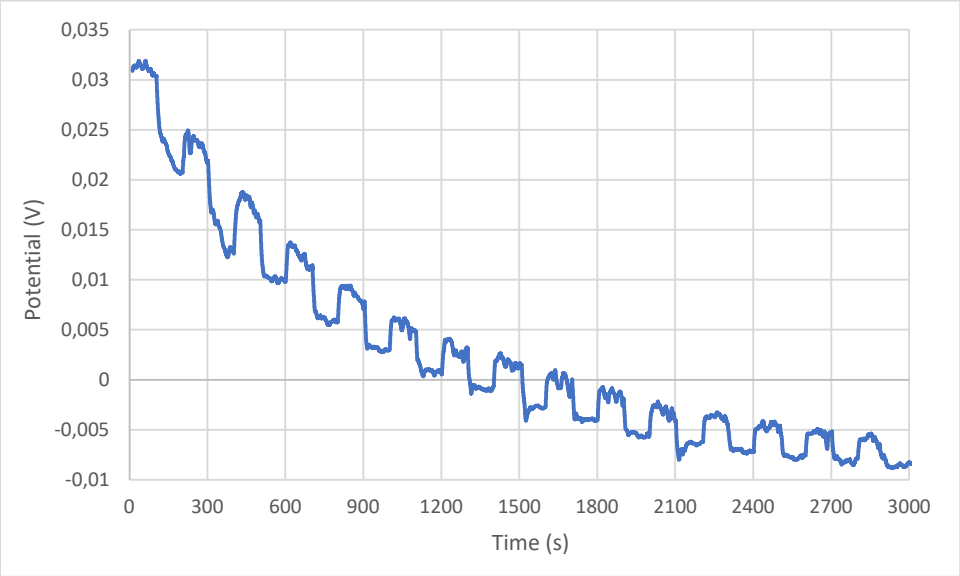

Figure 3.48. Chronopotentiometry of Sensor 13 in 0.1 M KCl.

The sensor works from the beginning and again is behaving the opposite as we were expecting. However, the measurement is good because the response to the light is fast and clear, and the peaks have high reproducibility. A decrease in the potential is observed from the first peak to the last and we can also observe a tendency of potential stabilisation in both processes (relaxation and excitation).

The main causes that could make the measurements go the opposite as we were expecting (potential increasing during excitation and decrease during relaxation), were either

the effect of the light incidence on the working electrode or well the effect of the light incidence over the Ag/AgCl reference electrode. The fact that both types of sensors (modification over the WE or modified ink) show this phenomenon, rules out the possibility that either of the two modifications is responsible. To try to find an explanation, we will carry out a measurement with the reference electrode covered, out of the incidence of light, and, in the middle of the procedure, we will uncover this electrode to see if the result changes. The intensity for the measurement is 25.63 Wm^{-2}.

Table 3.17. Incidence and non-incidence of light periods and light irradiance intensity.

No light incidence periods (s)	Light incidence periods (s)
-	0-100
100-200	200-300
300-400	400-500
500-600	-
Reference electrode is uncovered	
-	600-700
700-800	800-900
900-1000	1000-1100
1100-1200	-

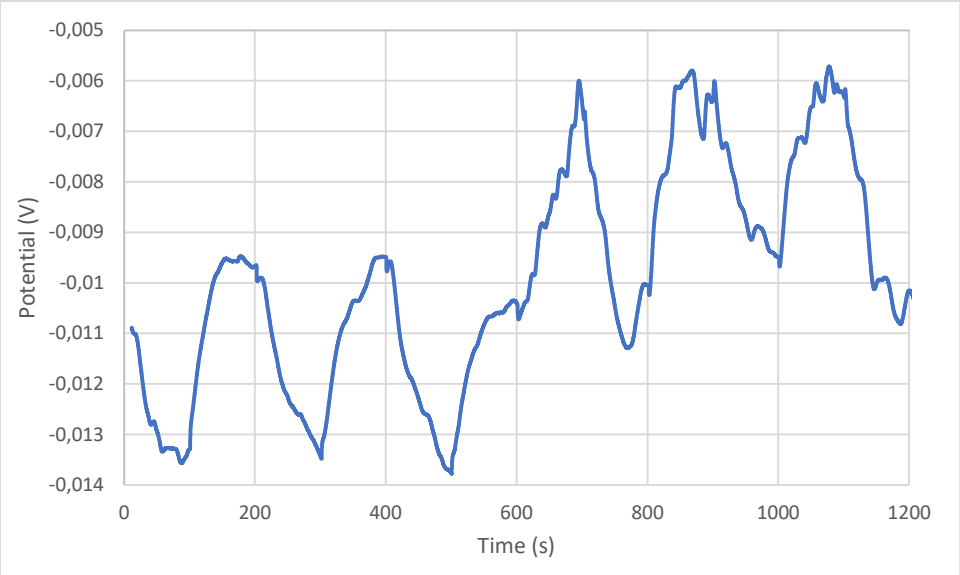

Figure 3.49. Chronopotentiometry of Sensor 13 with reference electrode covered in 0.1 M KCl.

From the beginning to the 600 seconds of measurement, we can observe that while the reference electrode is covered, the measurement happens as we were expecting in a normal case. From the moment that we uncover the electrode (600 seconds), it starts going the opposite way than normally, as in many of the last measurements. Thus, we conclude that the Ag/AgCl reference electrode is responsible for the anomalous behaviour of the sensor. To further study the influence of this interference, we performed a measurement with the same procedure, i.e. half chrono potentiometry with the reference electrode covered and the other half with the

electrode uncovered, but this time with Sensor 12, which had functioned normally without any lack of this variation. In this measurement, the intensity will also be 25.63 W m^{-2}.

Table 3.18. Incidence and non-incidence of light periods and light irradiance intensity.

No light incidence periods (s)	Light incidence periods (s)
-	0-100
100-300	300-400
400-600	600-700
700-900	900-1000
1000-1200	1200-1300
1300-1500	-
Reference electrode is uncovered	
-	1500-1600
1600-1800	1800-1900
1900-2100	2100-2200
2200-2400	2400-2500
2500-2700	2700-2800
2800-3000	-

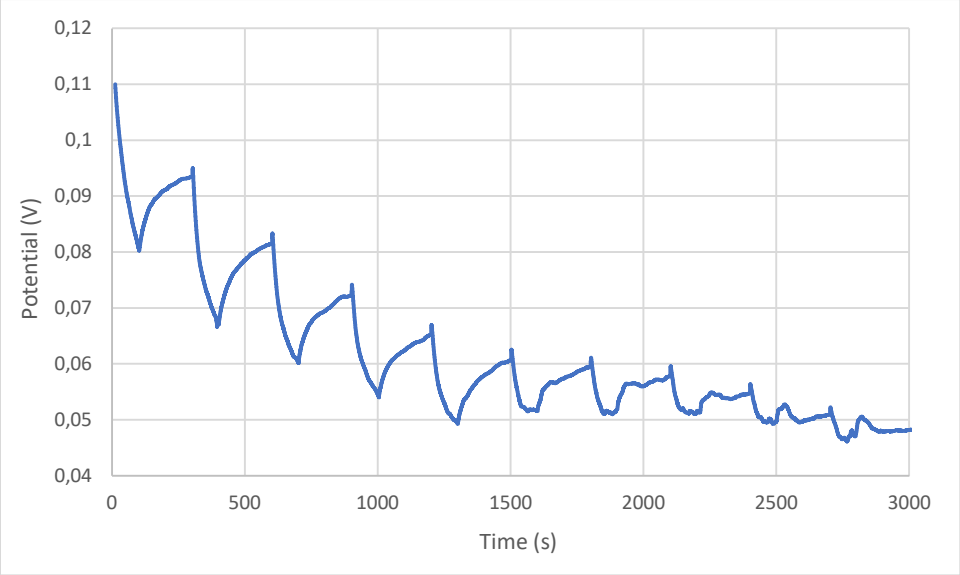

Figure 3.50. Chronopotentiometry of Sensor 12 with reference electrode covered in 0.1 M KCl.

We can observe that while the reference electrode is covered, the measurement happens perfectly with clear and not noisy peaks, and then, when the electrode is uncovered the measurement starts to get noisier and blurrier.

3.3.2. Current measurements

After testing all the sensors on the chronopotentiometry we are going to test the sensibility to electric current by the chronoamperometry technic. Now, the expected results are the opposite as before, the current should increase when the sensor is exposed to light incidence and decrease when it's not. The idea is to perform the measurement on all sensors except for Sensor 8, which did not respond to light incidence, and Sensor 13. The latter cannot be used due to the deterioration of its working electrode, which will also be considered when assessing its performance.

For these new measurements we have changed our electrolyte and now use a 0.1M KNO_3 solution. In addition, they are all taken with the reference electrode covered, to avoid any interference. We start with Sensor 7 again, which will be the only one of its kind where we will practice this type of measurements.

Table 3.19. Incidence and non-incidence of light periods and light irradiance intensity.

No light incidence periods (s)	Light incidence periods (s)	W m^{-2}
0-100	100-200	25.63
200-300	300-400	
400-500	500-600	
600-700	700-800	
800-900	900-1000	
1000-1100	1100-1200	1.80
1200-1300	1300-1400	
1400-1500	1500-1600	5.42
1600-1700	1700-1800	
1800-1900	1900-2000	25.63
2000-2100	2100-2200	

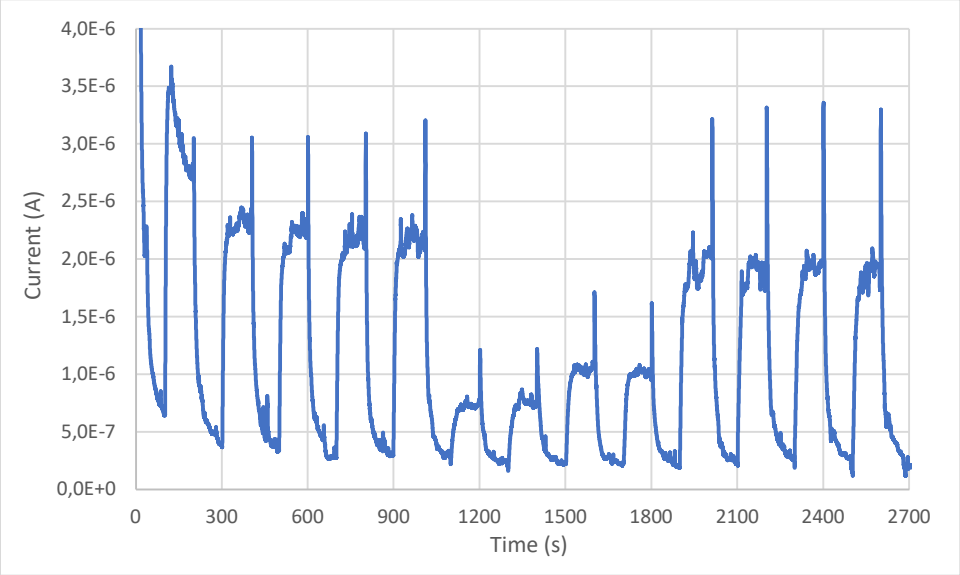

Figure 3.51. Chronoamperometry of Sensor 7 in 0.1 M KNO_3.

As we can observe, the sensibility of the sensor on electric current is better than for potential. The peaks are well distinguished, and the current tend to stabilise after increasing or decreasing to a certain level. We can also observe the influence of light incidence, as far is the sensor from the spotlight the lower became the current. After the stabilisation of the increasing current, just at the moment that the sensor is taken out of the spotlight, we can see a sudden rise in the current that instantly fall.

We move on to the other types of sensors starting with Sensor number 10.

Table 3.20. Incidence and non-incidence of light periods and light irradiance intensity.

No light incidence periods (s)	Light incidence periods (s)	W m^{-2}
0-200	200-300	25.63
300-400	400-500	
500-600	600-700	5.42
700-800	800-900	
900-1000	1000-1100	1.80
1100-1200	1200-1300	
1300-1400	-	

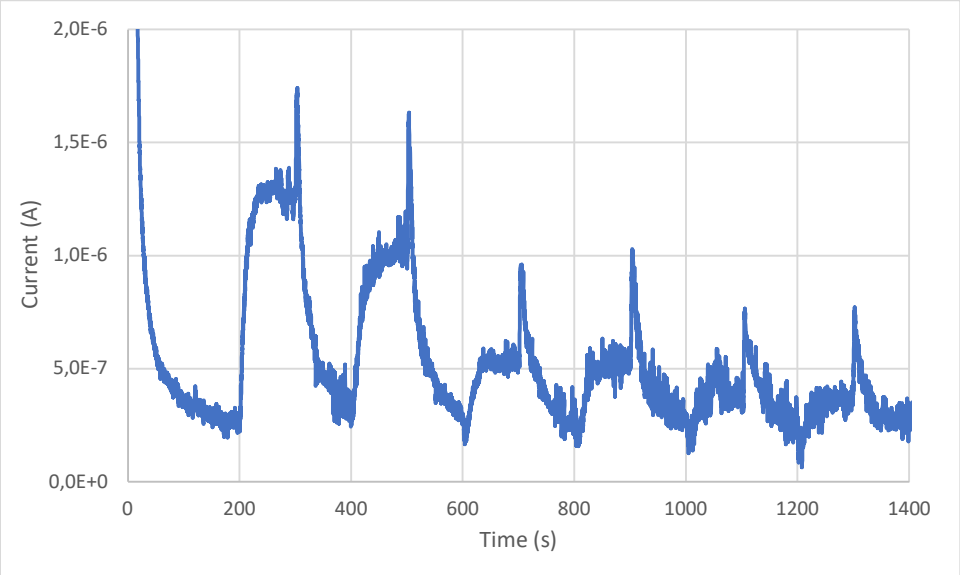

Figure 3.52. Chronoamperometry of Sensor 10 in 0.1 M KNO_3.

The sensor works properly from the beginning, but the current is way lower than the one obtained with the Sensor 7. At 10 cm we obtained a good measurement but from the moment that we put the sensor at 15 cm the signal obtained is too much affected by the noise. At 20 cm the signal is practically unnoticeable. The result is not bad, but it can be improved, that is why we repeat the measurement and this time we start from the lowest light intensity.

Table 3.21. Incidence and non-incidence of light periods and light irradiance intensity.

No light incidence periods (s)	Light incidence periods (s)	W m^{-2}
0-200	200-300	1.80
300-400	400-500	

500-700	700-800	5.42
800-900	900-1000	
1000-1100	1100-1200	25.63
1200-1300	1300-1400	
1400-1500	-	

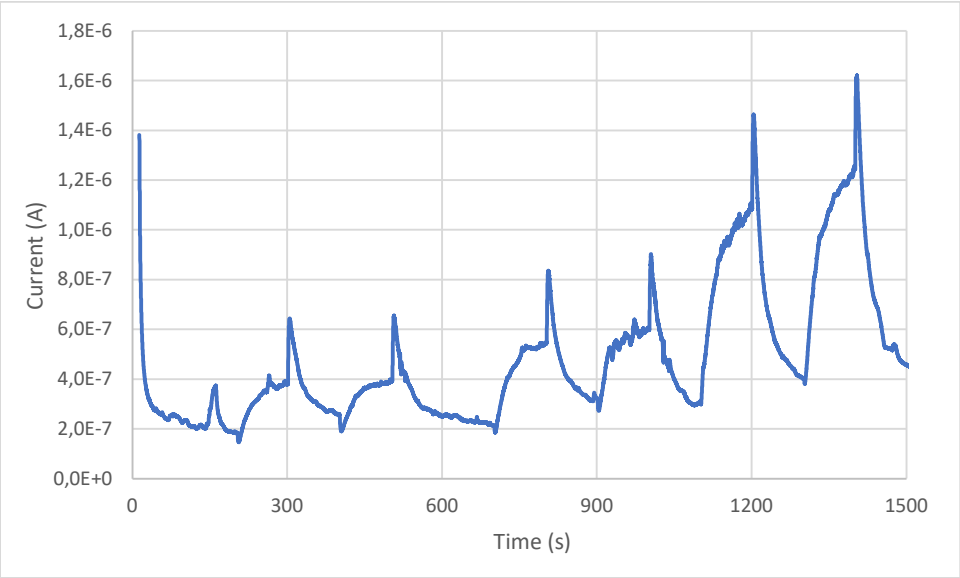

Figure 3.53. Chronoamperometry of Sensor 10 in 0.1 M KNO_3.

Similar result to the previous measurement, with the difference that this one is less affected by noise, the lecture at 20 cm can be distinguished easily. However, the signal is still way less than the one that we obtained with Sensor 7.

Table 3.22. Incidence and non-incidence of light periods and light irradiance intensity.

No light incidence periods (s)	Light incidence periods (s)	W m^{-2}
0-200	200-300	25.63
300-400	400-500	
500-600	600-700	5.42
700-800	800-900	
900-1000	1000-1100	1.80

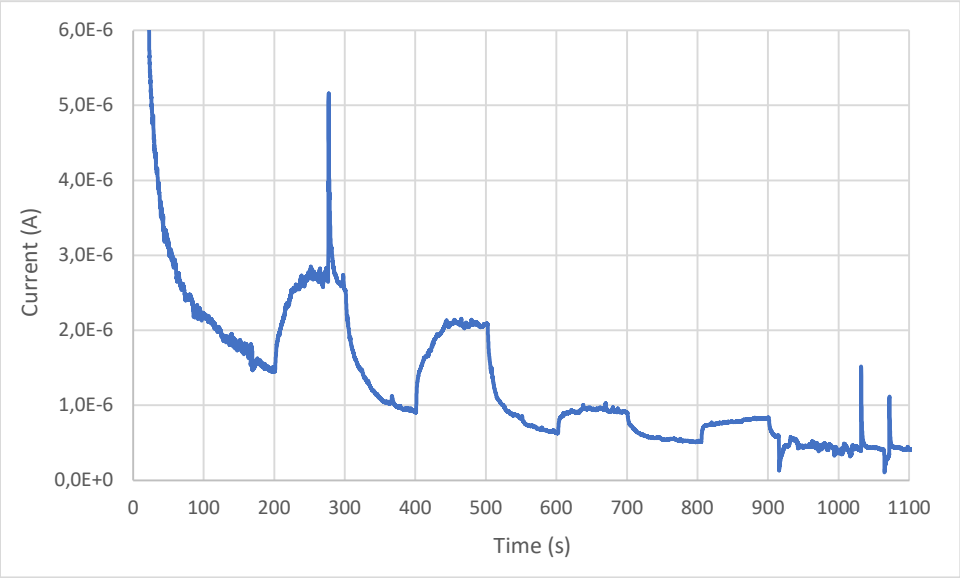

Figure 3.54. Chronoamperometry of Sensor 11 in 0.1 M KNO_3.

The response of this sensor is not as good at the one tried before. The signal is not as appreciable and at 20 cm is not able to give any significant response to the light incidence.

Lastly, we see the results obtained for Sensor 12.

Table 3.23. Incidence and non-incidence of light periods and light irradiance intensity.

No light incidence periods (s)	Light incidence periods (s)	W m^{-2}
0-200	200-300	25.63
300-400	400-500	
500-600	600-700	5.42
700-800	800-900	
900-1000	1000-1100	
1100-1600	1600-1700	1.80
1700-1800	1800-1900	
1900-2000	2000-2100	
2100-2200	-	

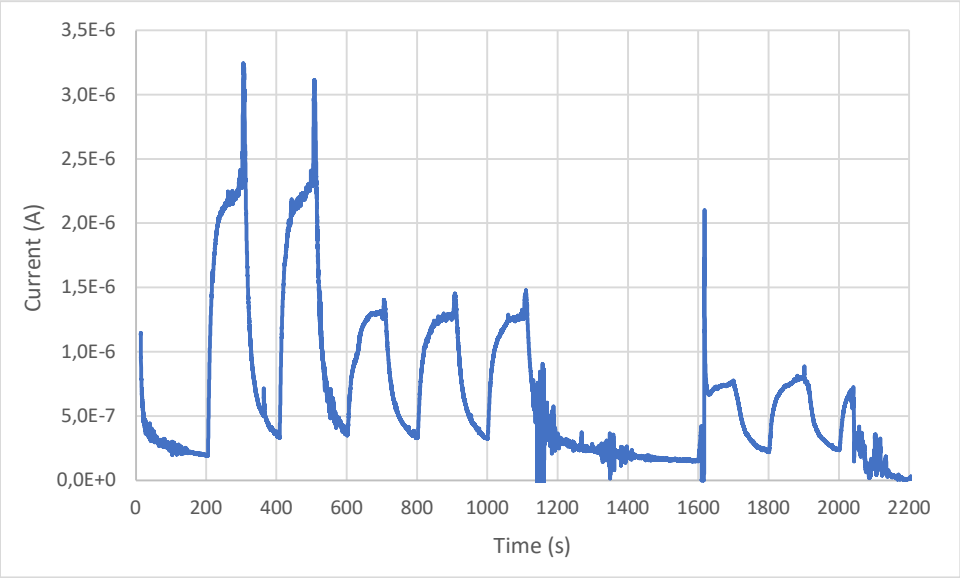

Figure 3.55. Chronoamperometry of Sensor 12 in 0.1 M KNO_3.

This sensor works as good as Sensor 7. We can see that the current obtained at the same distance from the spotlight are similar. The peaks are well distinguished, and as all the other current measurements, they tend to a stabilisation when they reach a certain level of current. The only issue with this measurement is that between 1100-1600 seconds there is a noisy spot. Then at 1600 seconds, it worked properly again, but at 2040 seconds the noise reappeared and we ended the measurement.

3.3.3. Result comparation

Now that we have all the results, we can compare them with each other. To determine which results are better, the speed of response to the stimulus and the sharpness, intensity, and reproducibility of the signal will be assessed. In addition, the durability of the sensor itself will also be considered.

Having said that, we will start by comparing the results of the sensors that had their modification on the reference electrode, i.e. numbers 7, 8, and 13. Since sensor number 8 did not give results, we exclude it from the comparison. We also excluded the measurement taken with Sensor 7 when the device was not immersed in the electrolyte solution. In order to be able to compare the results of both sensors, it will be necessary to adjust their results, as they occur in very different potential ranges. That is why, in order to compare them, we will equal their initial potentials, in this case, we will equal the potential of Sensor 13 with that of Sensor 7:

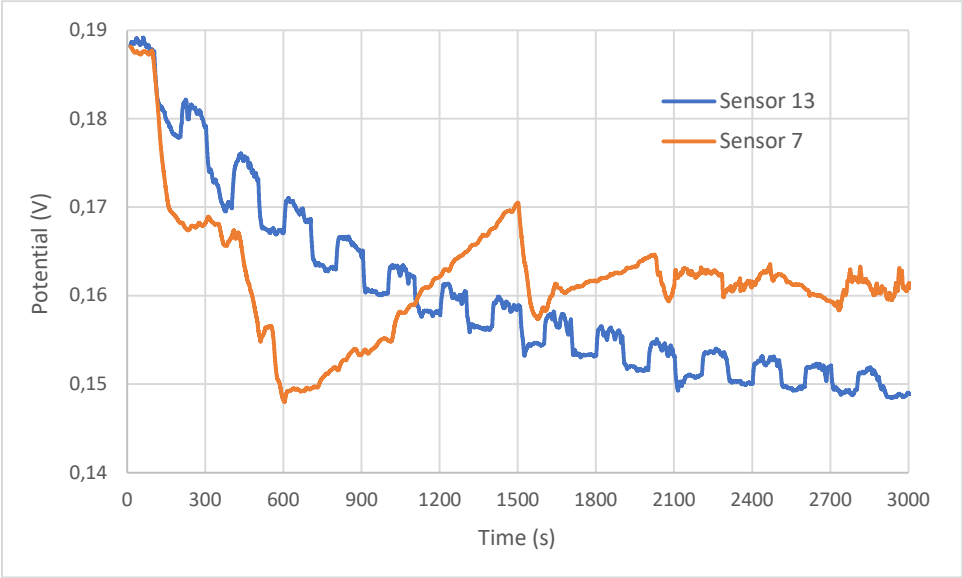

Figure 3.56. Chronopotentiometry comparation of sensors 7 and 13 in 0.1 M of KCl.

Even if the potentials are equal, these two results are difficult to compare, the main difference being the experience we had when taking the measurements (the measurement with Sensor 7 was taken first, while the measurement with Sensor 13 was from the last chronopotentiometry taken), so the conditions are not exactly the same. For Sensor 13 the luminous intensity is always 25.63 W m^{-2}, whereas, for Sensor 7, this luminous intensity is from 1500 seconds onwards (from 2020 onwards the luminous intensity is higher, 181.55 W m^{-2}). It can also be clearly seen that the result of Sensor 13 is much more reproducible, and its signal is sharper. As for the signal intensity, it is difficult to compare the two measurements, since due to the poor reproducibility of the peaks of Sensor 7, we cannot assign a value to it. We can therefore say that, for potential measurements, Sensor 13 offers more satisfactory results. On the other hand, we have the resistance of the device, which does not play in favour of Sensor 13.

Figure 3.57. Sensor 7 after use (left) and Sensor 13 after use (right).

Both pictures have been taken after 3 to 4 measurements of more than 3000 seconds under the spotlight, at most during half of the analysis. While Sensor 7 is still working normally, Sensor 13 is completely unusable. This is because of the silver corrosion, which delaminates the TiO_2 coating, making the sensor unusable.

Due to the low durability of Sensor 13, it was not possible to take measurements of electric current with this sensor, that is why for this type of sensor we only took them with Sensor 7. Therefore, its result will be the one that we will compare with the best result of the other type of sensors for the chronoamperometries.

We proceeded to compare the results of sensors 10, 11 and 12 with each other, which had different concentrations of TiO_2 in their ink (10%, 2% and 50% respectively). For this we take averages with the same light intensity, and for Sensor 11 we take the measurement with the longest duration. In this comparison, we will match the initial intensity of the analysis of Sensor 12 with that of Sensor 10, to make them easier to compare.

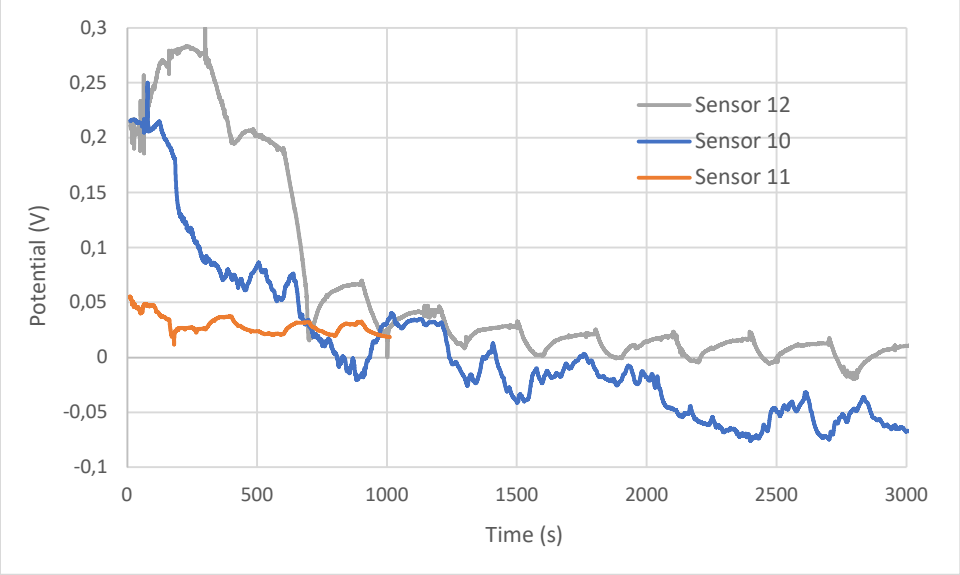

Figure 3.58. Chronopotentiometry comparation of sensors 12, 10 and 11 in 0.1 M KCl.

At a first glance we can already see that the signal of Sensor 11 is far below the other two. Therefore, we can discard its measurement. To get a better view of the results we will take a closer look at the results of sensor 10 and 12 by limiting the initial time to 600 seconds.

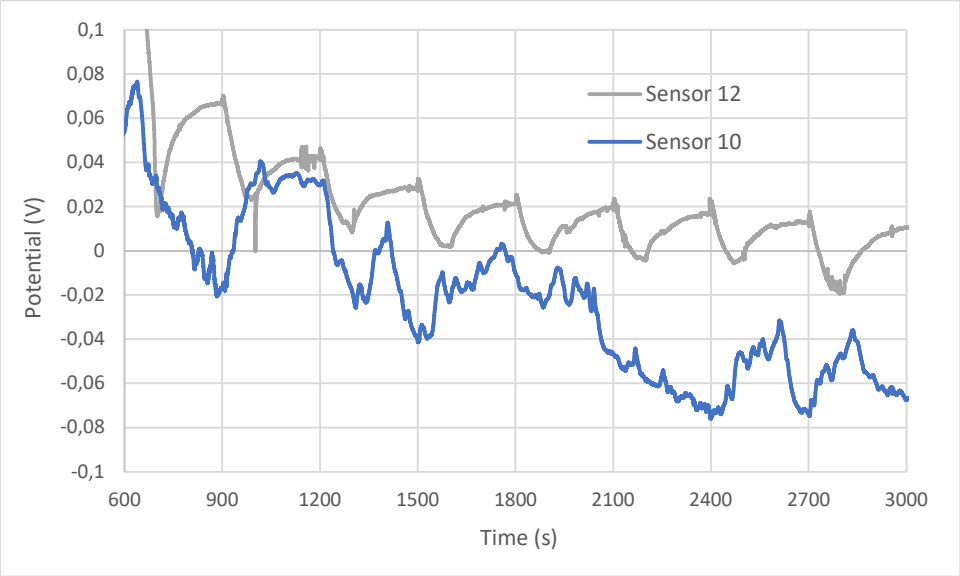

Figure 3.59. Chronopotentiometry comparation of sensors 12 and 10 in 0.1 M KCl.

Here we can clearly see that the result of Sensor 12 presents a sharper signal and more reproducibility in its peaks, making it the sensor with the best results of its type. That said, we can also conclude that the higher the amount of TiO_2 in the ink of the working electrode, the better the results, at least up to a concentration of 50% TiO_2.

We now compare the chronoamperometry results for these sensors, using the best of the results obtained for each.

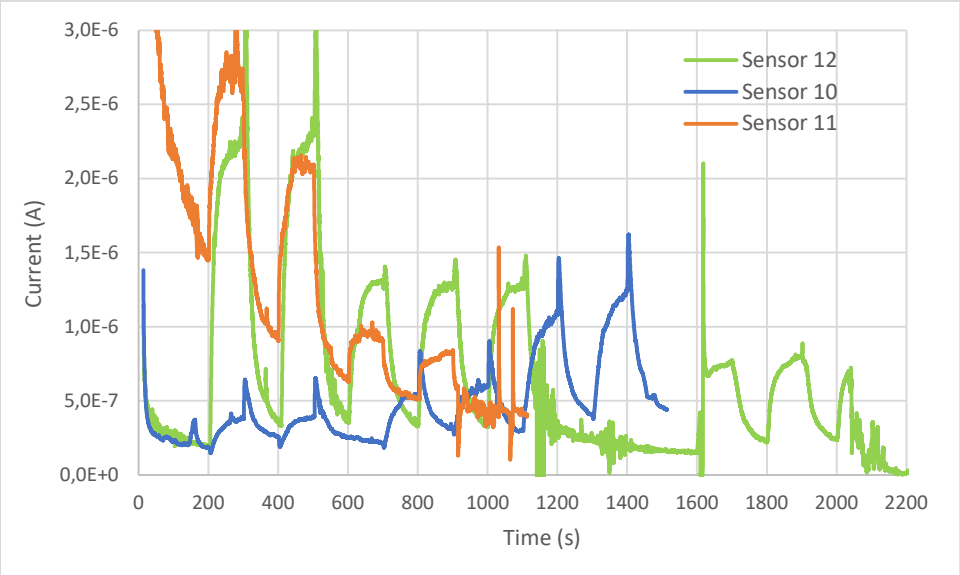

Figure 3.60. Chronoamperometry comparation of sensors 12, 10 and 11 in 0.1 M KNO_3.

First of all, we can discard Sensor 11, because even though its signal may appear to be higher than that of Sensor 10, it is the only one of the three sensors that is not able to work in the three different light intensities. To have a better view of the other two sensors, we present a graph of both results without the discarded sensor.

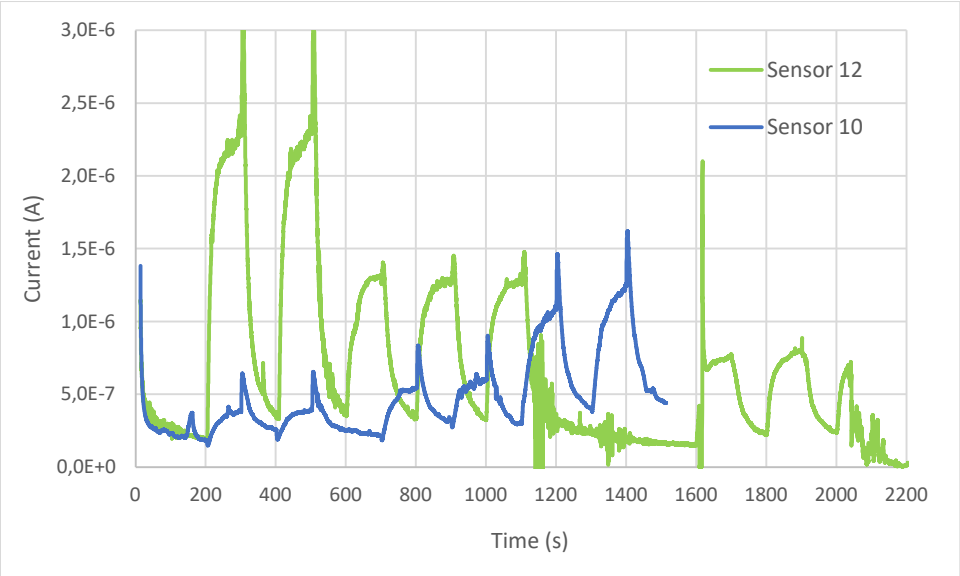

Figure 3.61. Chronoamperometry comparation of sensors 12, and 10 in 0.1 M KNO_3.

Both sensors can detect noticeable signals over the entire proposed intensity range. The measurement with Sensor 10 is sharper and less affected by sound. However, we consider the result obtained with Sensor 12 to be more satisfactory, due to the signal intensity of its peaks, which is almost double that of the other sensor. That said, as for the potentiometry results, this device is the one that gives the best results for detecting the electric current.

Finally, we compare the results of both types of sensors, starting with the results obtained in the chronopotentiometry, where we will compare the results of Sensor 13 and Sensor 12. To compare them, we adjust the results of Sensor 13, so we have equalised its starting point to the 678 seconds of the measurement of Sensor 12.

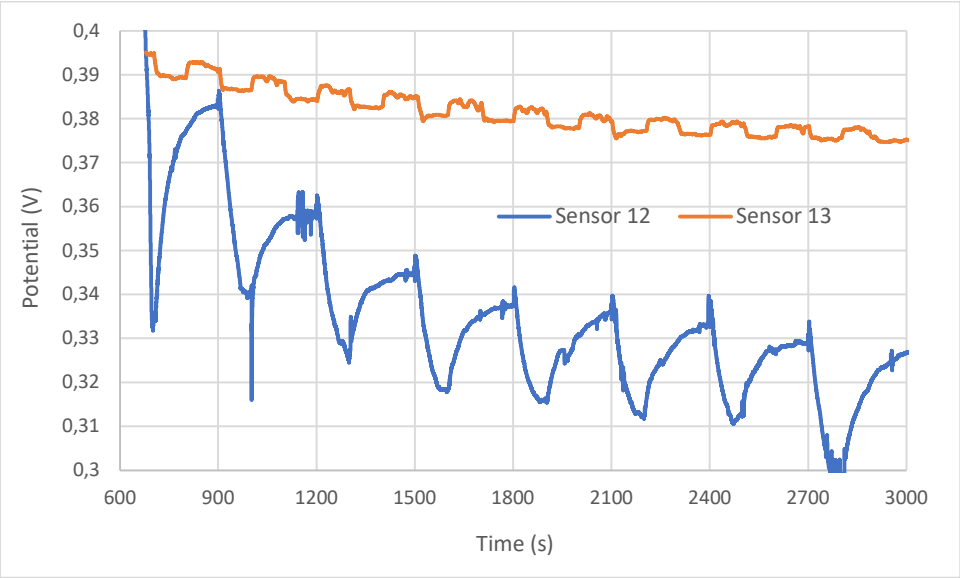

Figure 3.62. Chronopotentiometry comparation of sensors 12 and 13 in 0.1 M KCl.

In this graph we can see that the signal of the peaks obtained with Sensor 12 is much higher. In terms of the sharpness of the signal, Sensor 12 is probably also better, with only the reproducibility of its peaks being what makes Sensor 13 stand out. We can therefore conclude that of the two types of sensors, the one that has given the best results for electrical potential measurements is the sensor with a modified working electrode which includes a certain concentration of TiO_2 in its ink (in this case, specifically 50%).

For the comparison of chronoamperometry results we will use those of Sensor 7 and Sensor 12.

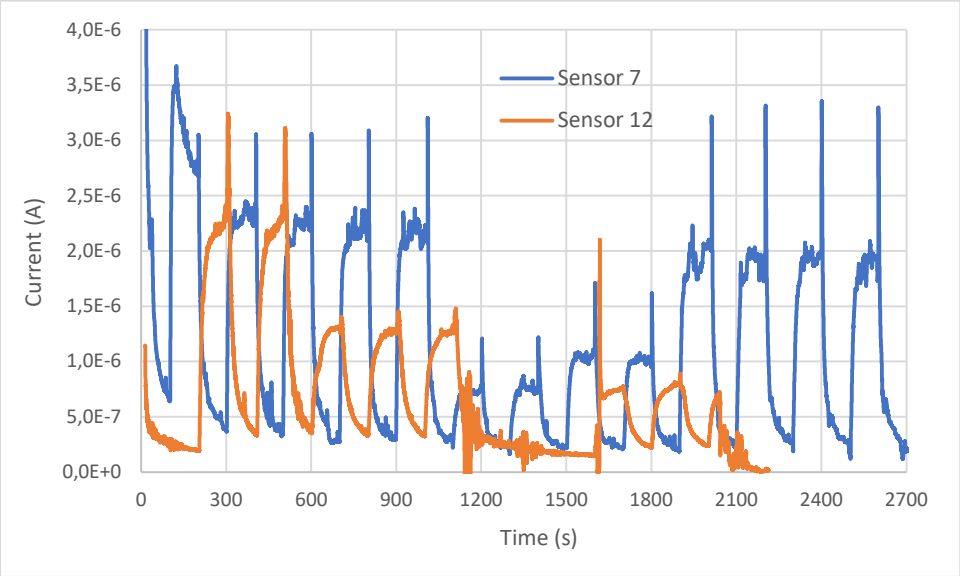

Figure 3.63. Chronoamperometry comparation of sensors 7, and 12 in 0.1 M KNO_3.

In view of the results, it is difficult to decide in favour of one of the two sensors. The signals obtained for the different light intensities are practically the same, as is the reproducibility of the peaks for both sensors. To position ourselves, we will point out that the measurement of Sensor 12 has sharper signals, especially at the point where the signal stabilises as the current increases. In this way, we establish that the best sensor for evaluating the electric current is Sensor 12.

With all the results and their comparison, the conclusion obtained is that the sensors with a modification in the ink of the working electrode work better than those with only a layer of TiO_2 covering it, both for potentiometric measurements and for electrical current measurements. It should also be noted that, for the latter parameter, the results obtained with Sensor 7 are practically as good as those obtained with Sensor 12, so its use in this field should not be ruled out either.

4. CONCLUSIONS

We have successfully achieved the goal of making a low-cost paper-based sensor that will give us satisfactory results. We have found a design that allows us to work even with the working area submerged, demonstrated that the device works for several electrochemical measurements, and in the present work, we have been able to direct its sensitivity towards air humidity and UV light through ink modifications. Even though we have not obtained good results for potentiometric measurements, we demonstrated that valuable information could be obtained with chronoamperometric methods. Future work should concentrate on formulations of inks with higher conductivity and on measurement protocols even more robust and less sensitive to the device resistance. There are two other issues, which are closely related: the size reduction of the sensor and the reproducibility of the manufacturing process. Although we have been able to manufacture sensors capable of working with electrolyte volumes of less than 200 µL, the fabrication process is too costly in terms of time and manufacturing success. To solve these problems, thinner templates should be used for these devices. In addition, a viable method to attach the stencils to the filter paper during electrode painting should be found, as the poor adhesion between them leads to ink leakage below the stencil relief, which in such small sizes almost always means that the entire device has to be discarded. Moreover, with smaller device sizes, even limited leakage can lead to low reproducibility. These improvements will materialize the potential of this kind of device as demonstrated by several contributions in the literature and by the present work, concerning the possibility to exploit the conductivity properties of the device and semiconductor modifications of the conductive ink.

5. REFERENCE AND NOTES

1. da Costa T.H., Song E., Tortorich R.P., Choi J.W. (2015). A paper-based electrochemical sensor using inkjet-printed carbon nanotube electrodes. *ECS Journal of Solid State Science and Technology,* 4(10), S3044-S3047.

2. de Tarso Garcia P., Garcia Cardoso T.M., Garcia C.D., Carrilho E., Tomazelli Coltro W.K. (2014). A handheld stamping process to fabricate microfluidic paper-based analytical devices with chemically modified surface for clinical assays. *RSC Adv*., 4, 37637-37644.

3. Oliveira A.E.F., Pereira A.C., de Resende M.A.C. (2022). Fabrication of Low-cost Screen-printed Electrode in Paper Using Conductive Inks of Graphite and Silver/Silver Chloride. *Electroanalysis*, 34, 1-11.

4. Tribhuwan Singh A., Lantigua D., Meka A., Taing S. Pandher M., Canci-Unal G. (2018). Paper-based sensors: emerging themes and applications. *Sensors,* 18, 2838.

5. Cinti S., Basso M., Moscone D., Arduini F. (2017). A paper-based nanomodified electrochemical biosensor for ethanol detection in beers. *Analytica Chimica Acta*, 960, 123-130.

6. Cinti S., Talarico D., Palleschi G., Moscone D., Arduini F. (2016). Novel reagentless paper-based screen-printed electrochemical sensor to detect phosphate. *Analytica Chimica Acta*, 919, 78-84.

7. Cinti S., Moscone D., Arduini F. (2019). Preparation of paper-based devices for reagentless electrochemical (bio)sensor strips. *Nature protocols*, 14, 2437-2451.

8. Cinti S., Fiore L., Massoud R., Cortese C., Palleschi G., Moscone D., Arduini F. (2018). Low-cost and reagent-free paper-based device to detect chloride ions in serum and sweat. *Analytica Chimica Acta*, 179, 186-192.

9. Tomei M.R., Cinti S., Interino N., Manovella V., Moscone D., Arduini F. (2019). Paper-based electroanalytical strip for user-friendly blood glutathione detection. *Sensors and Actuators B: Chemical*, 294, 291-297.

10. Fonseca W.T., Ribeiro Castro K., de Oliveira T.R., Censi Faria R. (2021). Disposable and flexible electrochemical paper-based analytical devices using low-cost conductive ink. *Electroanalysis*, 33, 1520-1527.

11. Oliveira A.E.F., Pereira A.C. (2021). Development of a Simple and Cheap Conductive Graphite Ink. *Journal of The Electrochemical Society*, 168, 087508.

12. Tai H., Duan Z., Wang Y. Wang S., Jiang Y. (2020). Paper-pased sensors for gas, humidity, and strain detections: A review. *ACS Appl. Mater. Interfaces*, 12, 31037-31053.

13. Zhao H., Zhang T., Qi R. Dai J., Liu S., Fei T. (2017). Drawn on paper: a reproducible humidity sensitive device by handwriting. *ACS Appl. Mater. Interfaces*, 9, 28002-28009.

14. Duan Z., Jiang Y., Huang Q., Wang S., Wang Y., Pan H., Zhao Q., Xie G., Du X., Tai H. (2021). Paper and carbon ink enabled low-cost, eco-friendly, flexible, multifunctional pressure and humidity sensors. *Smart Materials and Structures,* 30, 055012.